Layer-specific intracortical amplification shortens the lifetime of thalamocortical repetition suppression in primary auditory cortex

Thesis
for the degree of

doctor rerum naturalium (Dr. rer. nat.)

approved by the Faculty of Natural Sciences of Otto von Guericke University Magdeburg

by M.Sc. Jing Ma

born on 22.01.1989 in Hunan, China

Examiners: PD. Dr. Reinhard König
Prof. Dr. Manfred Kössl

submitted on 28th June 2021

defended on 5th May 2022

Summary

Layer-specific intracortical amplification shortens the lifetime of thalamocortical repetition suppression in primary auditory cortex

Author: *Jing Ma*

Keywords: *auditory adaptation, granular and infragranular layers, electrophysiology, $GABA_A$-agonist muscimol, regular-SOI paradigm, Mongolian Gerbil, current source density analysis*

Cortical adaptation has been suggested to be inherited from subcortical sensory pathways, to rely on synaptic depression of the thalamocortical synapse, to be influenced by intracortical balance between excitation and inhibition, and to be modulated by corticofugal feedback. In this PhD thesis, the goal was to disentangle intracortical from subcortical contributions to cortical adaptation. I have investigated repetition suppression (RS) as a fundamental aspect of adaptation in the primary auditory cortex (A1) of anesthetized of Mongolian gerbils (*Meriones unguiculatus*), and presented the regular-SOI paradigm with systematically varying stimulus onset intervals (SOIs) to create steady state adaptation at different strengths. Layer-specific analysis of synaptic mass inputs into the cortex was performed using current source density (CSD) analysis. To study the effect of intracortical synaptic input to adaptation, the intracortical processing was silenced with the $GABA_A$-agonist muscimol.

The major findings show that initial granular and infragranular sinks display different RS kinetics. Lifetime of the infragranular sink was nearly twice as long as that of the granular sink. Pharmacological silencing the intracortical processing had different impacts on the RS kinetics in both layers, which prolonged the lifetime of granular sink and did not change that of infragranular sink thus left comparable lifetime in both layers. These results demonstrate an intracortical contribution to RS in the granular layer, and raise the supposition of an intracortical mechanism that re-amplifies the suppressed thalamocortical inputs. Furthermore, it was shown for the first time that RS was stronger for the sink activity than for the sink integral, indicating an important role of synchronization of synaptic events in cortical RS.

Zusammenfassung

Schichtspezifische intrakortikale Verstärkung verkürzt die Dauer der durch wiederholte Stimulation erzeugten thalamokortikalen Response-Unterdrückung im primären auditorischen Kortex

Autorin: *Jing Ma*

Schlüsselwörter: *auditorische Adaptation, granuläre und infragranuläre Schichten, Elektrophysiologie, $GABA_A$-Agonist Muscimol, Regular-SOI-Paradigma, mongolische Wüstenrennmaus, Stromquellendichte-Analyse*

Kortikale Adaptation kann auf mehrere Ursachen zurückgeführt werden. So wird angenommen, dass sie von subkortikalen sensorischen Bahnen übernommen wird, von der synaptischen Unterdrückung der thalamokortikalen Synapse abhängt, vom intrakortikalen Gleichgewicht zwischen Erregung und Hemmung (Inhibition) beeinflusst wird und durch kortikofugale Rückkopplung moduliert wird. Ziel dieser Doktorarbeit war es, intrakortikale von subkortikalen Anteilen an der kortikalen Adaptation zu differenzieren. Hierzu habe ich die durch wiederholte Stimulation hervorgerufene Unterdrückung des auditorischen Responses ('repetition suppression' -- RS) als einen grundlegenden Aspekt der Adaptation im primären auditorischen Kortex (A1) von anästhesierten mongolischen Wüstenrennmäusen (Meriones unguiculatus) untersucht. Als experimentelles Paradigma habe ich das Regular-SOI-Paradigma mit systematisch variierenden Stimulus-Onset-Intervallen (SOI) eingesetzt, um eine Steady-State-Adaptation unterschiedlicher Stärke zu erzeugen. Eine schichtspezifische Analyse des synaptischen Masse-Eintrags in den Kortex wurde mit Hilfe der Stromquellendichte-Analyse ('current source density', CSD) durchgeführt. Um den Effekt des intrakortikalen synaptischen Inputs auf die Adaptation zu untersuchen, wurde die intrakortikale Verarbeitung mit dem $GABA_A$-Agonisten Muscimol ruhiggestellt.

Das zentrale Ergebnis meiner Arbeit ist der Befund, dass initiale granuläre und infragranuläre Senken unterschiedliche RS-Kinetiken aufweisen. Die Lebensdauer der infragranulären Senke war fast doppelt so lang wie die der granulären Senke. Die pharmakologische Unterdrückung der intrakortikalen Verarbeitung hatte unterschiedliche Auswirkungen auf die RS-Kinetik in beiden Schichten: sie führte zu einer Verlängerung der Lebensdauer der granulären Senke, während sich die Lebensdauer der infragranulären Senke nicht veränderte, was wiederum vergleichbar lange Lebensdauern in beiden Schichten zur Folge hatte. Die Ergebnisse meiner Arbeit zeigen einen intrakortikalen Beitrag zur RS in der granulären Schicht und lassen einen intrakortikalen Mechanismus vermuten, der die unterdrückten thalamokortikalen Inputs erneut verstärkt. Darüber hinaus wurde zum ersten Mal gezeigt, dass RS für die Senken-Aktivität stärker war als für das Senken-Integral, was auf eine wichtige Rolle der Synchronisation von synaptischen Ereignissen bei der kortikalen RS hinweist.

Contents

List of Figures

List of Tables

Abbreviation

1. Introduction

This chapter starts with a brief discussion of the functional principle of the sensory systems—which have been refined by evolutionary selection—to efficiently, but not perfectly, transmit and process inputs in a way that enhances survivability. As a pervasive phenomenon, a broad definition of sensory adaptation refers to the capability of the sensory system to vary its response properties according to the changing statistics of stimulation, in achieving efficient coding. During research, various coding strategies are identified by its corresponding stimulus statistics. A simple example of stimulus statistics is a set of rare stimuli being embedded in a set of frequent stimuli, the gradual decay of response strength to the frequent stimuli is defined as sensory adaptation or neural adaptation. Then the auditory adaptation is discussed by relating anatomical properties of the central auditory system and several marked forms of auditory adaptation, i.e. mismatch negativity, stimulus specific adaptation and repetition suppression. Finally the discussion covers the scope and objectives of this dissertation, which is the cortical shaping of auditory adaptation.

1.1 Sensory adaptation from an evolutionary perspective

Sensory systems are the products of hundreds of millions of years of evolution. They are often closely linked to the ecology of a species, and have been shaped by an array of selection pressures to enable an animal to perform numerous behaviors. In short, sensory systems are fundamental to survival and reproduction and shape much of evolution and behavior. Animals should, and do, only pay attention to features of the habitat that are important to them. What they can detect and respond to is dictated by their sensory systems and how they are constructed over evolution.

— Martin Stevens[1]

Animal behavior can be considered as a series of choices and decisions, based on simultaneous and constant estimation of their sense of the immediate surroundings (Phelps, 2007). The sensory nervous system is responsible for sensation with transmitting information

[1] *Stevens, Martin. Sensory Ecology, Behavior, and Evolution. First Edition. Oxford: Oxford University Press, 2013.*

from the surrounding physical world to the internal system, as well as processing and modifying the information in order to serve perception and behavior (Krantz, 2012). As a result of evolution, both sensory system and animal behavior are constrained by survival and reproduction. Thereby, the sensory system does not perfectly replicate the environment, but rather recreates a functioning model of the real world. This model is designed in an efficient and meaningful way, to serve the purpose of survival and reproduction of an individual and the species (Krantz, 2012).

Beyond the lifetime of a single individual, a conceptual framework of sensory ecology considers how the sensory system has been elaborately constructed to extract meaningful information out of complex surroundings, while leaving out the irrelevant information (Phelps, 2007). To deal with the excess of environmental information, the sensory system is constantly adjusting its responses to encode the inputs whose statistics vary in time (Wark et al., 2007). Through ongoing recalibration, sensory system economically allocate its sensory receptors and computational resources in order to maximize the performance in a relevant task, while remaining sensitive to unexpected changes in the environment (Webster, 2012). In general, these rapid sensitivity adjustments are known as sensory adaptation, i.e. changes in the response features of sensory modalities induced by the recent stimulus context. Hence, an important implication is that much of the ongoing stimulus processing is affected by the preceding input (Webster, 2012).

1.2 General functions of sensory adaptation

Sensory adaptation has been robustly shown across a variety of sensory modalities (vision, audition and touch) and at different levels (peripheral and central) of sensory processing (Webster, 2012). Depending on the specific stimulus context, sensory adaptation occurs in various forms, such as enhanced or diminished sensitivity towards the targeting stimulus. Well known examples are light-dark adaptation (Gouras, 1972), olfactory adaptation (Köster & de Wijk, 1991), and taste/gustatory adaptation (Bujas et al., 1995). In perceptual science, it has been documented how sensory adaptation leads to certain perceptual 'after-effects', such as perceptual illusions. For instance, after viewing tilted lines for some time, bias on what looks vertical can occur (Gibson, 2004).

In pursuing to gain an understanding of different types of sensory adaptation, researchers

categorize them by the corresponding statistic properties of the stimuli. The simplest example of a changing distribution of the stimulus probability is a sequence of stimuli that contains two different stimuli, with one stimulus occurring more frequently than the other. In this scenario, the sensory system may adapt to the frequent stimulus with a gradually decaying responsiveness while it responds stronger to the rare stimulus (Wark et al., 2007). This gradual decrease of the responsiveness of the sensory system towards the frequent stimuli is defined as neural adaptation or sensory adaptation (Chung et al., 2002). In the current study, I will be focusing on this specific sense of adaptation, namely, neural adaptation. Furthermore, the term neural adaptation was chosen and will be used in the following text to distinguish it from the broader definition of sensory adaptation that has been introduced above.

There exist a multitude of theories addressing the functional importance of neural adaptation that are not necessarily mutually exclusive. Neural adaptation has been assumed to enhance the limited neural response range to encode sensory inputs with much larger dynamic ranges by shifting the range of stimulus amplitudes, thus acting as a spectrotemporal contrast gain control mechanism (Chung et al., 2002; Rabinowitz et al., 2011). Given the reduction of response level and awareness of a constant stimulus, neural adaptation allows to free up neural resources and attention to attend to other more important inputs like detecting stimulus changes (Puccini et al., 2006; Ulanovsky et al., 2003). It is also suggested to be significant for the deviance detection, predictive coding and sensory memory (Nelken, 2004, 2014; Winkler et al., 2009).

1.3 Auditory adaptation and its research dimensions

Sensory adaptation is particularly well investigated in the auditory system. This is presumably due to the importance of stimulus timing, sequencing, and streaming, or more general, of the temporal statistics of the input in auditory processing (Malmierca et al. 2014; Pérez-González and Malmierca 2014). It has been suggested that the auditory adaptation plays an important role in the integration of sequential acoustic information, in the formation of sensory memory (Lu et al., 1992), as well as in detecting unexpected stimuli so to determine its survival relevance (Malmierca et al., 2014). With the advancement of measuring technology of neural activities, auditory adaptation has been extensively investigated in recent decades with fascinating progress in terms of its various sub-forms, experimental paradigms, and scales of

observation (Pérez-González and Malmierca 2014). Aiming to provide an overview on these relevant issues as well as narrowing down the scope of the current research object—cortical contribution to the repetition suppression (RS) —several interrelated sub-forms of auditory adaptation will be briefly introduced, with the additional intention to invoke certain cautiousness in citing and comparing across auditory adaptation research. Firstly, I will start with the discovery and challenges of the mismatch negativity (MMN), which has classically received a lot of interest due to its link to various cognitive functions and clinical applications. In the search of the cellular correlates of MMN, stimulus specific adaptation (SSA) serves as a strong candidate. Finally, RS will be discussed as the fundamental formation process of SSA.

1.3.1 Mismatch negativity as an important indicator for cognitive phenomenon

MMN and its cognitive as well as clinical importance

Magnetoencephalography (MEG) and electroencephalography (EEG) are non-invasive technique in measuring neural responses in the brain with excellent temporal resolution. MMN (Figure 1.1) categorizes the enhanced strength of event-related magnetic fields or electric potentials that typically appear in response to an unexpected or rare stimulus embedded in a repetitive sequence of expected or regular (frequent) stimuli in the post-stimulus latency range between 100 and 200 ms (Näätänen et al., 1978). MMN appears robustly across sensory domains and has been mostly studied in vision and hearing (Fitzgerald & Todd, 2020; May & Tiitinen, 2010; Michie et al., 2016a; Pazo-Alvarez et al., 2003).

As an indirect index of change detection, MMN's importance has been growing in the past decades since it has been suggested to be responsible for various cognitive phenomena like auditory sensory (echoic) memory (May & Tiitinen, 2010), predictive coding (Fong et al., 2020), perceptual learning (Fitzgerald & Todd, 2020), and musical processing (Tervaniemi, 2001). Clinically, MMN has been used as an objective indicator for various neuropsychiatric conditions, for example, attention deficit hyperactivity, auditory extinction, Parkinson's disease, and, especially, schizophrenia (Michie et al., 2016a; Näätänen et al., 2012). The reduction of the amplitude of MMN has been considered a highly replicable biomarker in schizophrenia patients (Michie et al., 2016b).

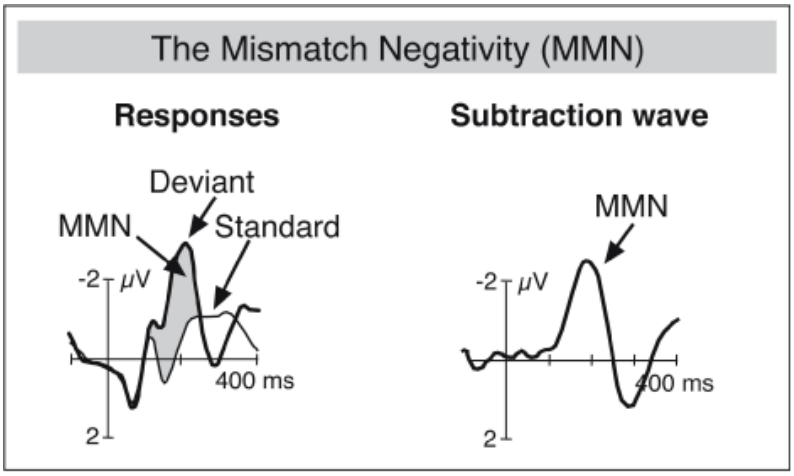

Figure 1. 1 Schematic illustration of the mismatch negativity (MMN)

Left, the thin waveform represents brain response towards standard/ frequent stimulus and the thick waveform that to deviant/ rare stimulus. The shading area is the difference between the two thus the MMN. **Right**, the MMN is more clearly shown with the subtraction wave. *(Original figure from Kujala & Näätänen, 2001 and was adapted by Friederici, A. 2009*)

MMN has been typically induced and tested with the oddball paradigm (Figure 1.2A, Somani & Shukla, 2012), during which a small portion of a deviant stimulus is randomly embedded in a train of identical and standard stimuli (Squires et al., 1975). It has been shown that the deviant stimuli with change in one or several of the characterizing features (e.g. audio frequency, duration and intensity et al.) is able to trigger a fresh response, namely, MMN. Additionally, a paradigm specific oddball variant, the switching oddball paradigm (Figure 1.2B, Ulanovsky et al., 2004), has been developed to eliminate potential stimulus-dependent effects. In this approach, in separate parts or sessions of the measurement, two stimuli are presented with reversed roles of being either standard or deviant.

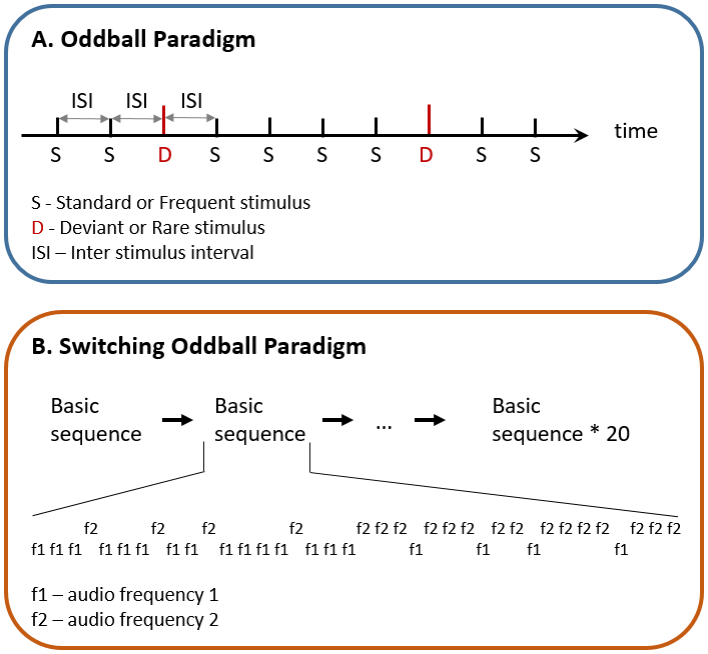

Figure 1. 2 Schematic illustration of the oddball paradigm and the switching oddball paradigm

(*adapted from Somani & Shukla, 2012 and Ulanovsky et al., 2004*). **A. Oddball paradigm**, during a train of stimuli, the deviant stimuli are randomly and infrequently embedded in a sequence of frequent and standard stimuli. The deviant and the standard only differ in one of the characterizing features like frequency, intensity, duration, and so on. All stimuli are presented with equal inter-stimulus interval (ISI). **B. Switching oddball paradigm**, the whole stimulation consists of multiple basic sequences. In each basic sequence of the example shown here, standard and deviant tones differ in their audio frequency. In the first half of the stimulus train, the frequency f1 is frequently presented as standard and the frequency f2 is infrequently and randomly presented as deviant. In the second half of the paradigm, the roles of both stimuli have been reversed with f1 now being the deviant and f2 being the standard.

The neuronal basis of MMN –debate and challenges

The neurobiological basis of MMN has been under a veil for several decades. Two popular candidates are the memory-based model (Näätänen et al., 1978, 2007) and adaptation model of MMN (May & Tiitinen, 2010; May & Tiitinen, 2001; Ulanovsky et al., 2003). The memory-based model assumes a comparing mechanism between the incoming auditory stimuli of its specific properties such as intensity, duration, frequency, etc., with the properties of the preceding stimulus stored in memory. In case of a mismatch between consecutive stimuli, a MMN response is generated. On the other hand, the adaptation model suggests that the frequently presented standard stimuli lead to the suppression or adaptation of those cells that are tuned to it, whereas the deviant stimulus then evoke the non-adapted 'fresh afferents' that contribute to an enhanced MMN response. Although the memory-based model has been

widely used since decades, several critical questions remain: What is the physiological mechanism of the stored memory trace? How does the comparison process exactly work? How does the system generate MMN? (May & Tiitinen, 2010)

The neural correlates of MMN have been closely examined by invasive measurements taken in animal models. In order to achieve the highest level of translational validity, certain criteria needed to be identified, and methodological issues had to be considered to capture and select a 'true', human-like MMN in an animal model. A major challenge in identifying the neuronal correlates of MMN is the lack of a solid link between observations at different measurement scales. Specifically, what are the counterparts of MMN in the measurements at the meso- and microscopic level of electrophysiology, single cell recordings, etc.? The mismatch response recorded in diverse measurements shows various response properties in terms of polarity, latency, or duration of the response, different level of response shift towards deviant stimuli, as well as their sensitivity to changes in characters of the deviant and ISI (Harms et al., 2016). Moreover, different measurement techniques have their own favored subjects and states of manipulation, thus causing further complications (Harms et al., 2016). Neural correlates of MMN have been studied in a range of animal species like mice, rats, cats, and primates (Javit et al., 1994; Pérez-González et al., 2005; Ulanovsky et al., 2003, 2004; Umbricht et al., 2005). The majority of these studies demonstrated the presence of SSA, for its larger response to the deviants over the standards, characterizing it as a candidate of the cellular correlate of MMN.

1.3.2 Stimulus specific adaptation as a potential neural basis of MMN

Stimulus specific adaptation has been widely observed and its similarity to MMN

SSA refers to the specific reduction in the neural activity towards a frequent repetitive ('standard') stimulus, while this reduction does not (or only partially) generalize to rare ('deviant') stimulus (Pérez-González & Malmierca, 2014; Taaseh et al., 2011), which is typically tested with oddball and switching-oddball paradigms. SSA has been reported in various animals models including birds, cats, rodents, and monkeys with several different recording techniques such as single-, multi-unit recordings, and local field portentials (LFPs) (Hershenhoren et al., 2014; Javit et al., 1994; Lu & Vicario, 2011; Ulanovsky et al., 2003, 2004). Empirical evidence has revealed certain similarities between SSA and MMN (Nelken & Ulanovsky, 2007). The magnitudes of MMN and SSA both increase with deviant rarity (Ulanovsky et al., 2004; von der

Behrens et al., 2009), parametric difference between standard and deviant, for example, the frequency separation between them (Näätänen et al., 1978; Ulanovsky et al., 2004). They both reveal long time constants of seconds or tens of seconds (Ulanovsky et al., 2003, 2004). Longer inter-stimulus interval (ISI) decreases both MMN and SSA, and they are both observable in the auditory cortex (AC), see Fishman & Steinschneider, 2012; May & Tiitinen, 2010; Ulanovsky et al., 2003. Therefore, SSA has been proposed as a strong candidate of being the cellular substrate of MMN.

Interactive multi-processing of SSA along the central auditory pathway

In empirical studies searching for the neural correlate of SSA, neurons exhibiting SSA were found at different levels along the central auditory pathway (Harms et al., 2016). In the IC of anesthetized rats, SSA to pure tones has been observed (Duque et al., 2012; Malmierca et al., 2009; Zhao et al., 2011). In the next auditory station, the medial geniculate body (MGB), extracellular recordings of single- and multiunits revealed SSA in all of its three main subnuclei ventrial (MGv), medial (MGm), and dorsal (MGd) in mice (Anderson et al., 2009) and rats (Antunes et al., 2010). Moreover, LFP recordings reported SSA in the rat AC (Szymanski et al., 2009; Taaseh et al., 2011). Given the highly hierarchical and interactive nature of the auditory system, these observations trigger questions like whether there is a single generator of SSA projecting its outcome to the rest of the network, or whether there are parallel and hierarchically organized processes contributing to sensory adaptation. Further, how does SSA develop and evolve among the auditory pathways and network? And what is the functional role of each network node in terms of information coding and processing?

Auditory information is transmitted ascendingly from inferior colliculus (IC) via MGB to the AC (Winer & Schreiner, 2005), in parallel through the more narrowly tuned lemniscal pathway and the more broadly tuned non-lemniscal pathway (Carbajal & Malmierca, 2018), meanwhile, the cortex is sending down stream feedback as a contral of certain subcortical stations via corticofugal system (Suga et al., 2000; Winer, 2005). Thereby, functional interaction among different auditory stations in processing SSA have drawn considerable attention. Extracellular measurments with rats by Zhao et al. (2011) showed a higher percentage of neurons exhibiting SSA in the IC than in the AC, wheares AC neurons adapted at a stronger level than IC neurons in terms of averaged response amplitude. Along the lemniscal pathway, SSA has been shown only until the AC, but not at the subcortical level, whereas it has been widely observed among

subcortical stations along non-lemniscal pathway (Carbajal & Malmierca, 2018). Exhilaratingly, Bäuerle et al. (2011) managed to reduce the SSA in the MGv via pharmacological inactivation of the AC with muscimol in Mongolian gerbil. This was the first demonstration of SSA observed in MGv being controlled by the corticofugal system. Therefore, the AC could possibly cause adaptive control on the subcortical structures and lead to the adjustment of its own input depending on the processing context (Bäuerle et al., 2011). These suggest that different forms of SSA exist in parallel, at different stages of auditory processing. However, in a network, SSA at different auditory sites will not be independent from each other. How the different forms of SSA interact, however, is an open question. It is still unclear whether the AC merely inherite adaptation from thalamocortical inputs or whether it contributes its own manupulation on the inheritage and then send the computational output downwards as a cortical control of the subcortical stations (Bäuerle et al., 2011; Malmierca et al., 2015).

1.3.3 Repetition suppression – looking into the formation process of SSA

Definition and its stimulus-onset interval dependence

Neuronal repetition suppression (Mayrhauser et al., 2014) or RS terms the attenuated neural responses towards repetitive stimuli (Auksztulewicz & Friston, 2016; Garrido et al., 2009; Utzerath et al., 2017), as presented in Figure 1.3. Thus, RS is considered as the fundamental aspect of auditory adaptation in all its forms like MMN, SSA, due to the reduction of the neural response with the frequently repeated presentation of a stimulus.

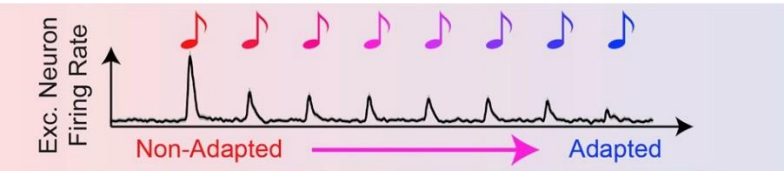

Figure 1. 3 Adaptation of neuronal responses to repeated sounds (Natan et al., 2017)

Similar to SSA (Malmierca et al., 2009; Zhao et al., 2011), the attenuating speed of the evoked response along a repetitive stimuli train and the level of RS have been shown to be sensitive to ISI and stimulus-onset interval (SOI) (Zacharias et al., 2012). These features have been previously tested with the regular-SOI paradigm (Figure 1.4), in which repetitive stimuli were presented with a particular constant SOI within a certain block, and the SOI being varied

across blocks. The shorter the SOI, the faster and the more the response is suppressed. Notably, RS needs time to build up. After a settling phase, neural responses amplitudes decay until they reach a plateau. Once a stimulus block has finished, the response can fully recover when given a long enough pause. RS involves both suppression and recovery processes that are both influenced by the SOI value. The plateau phase of RS marks a steady state in which suppression and recovery are balanced.

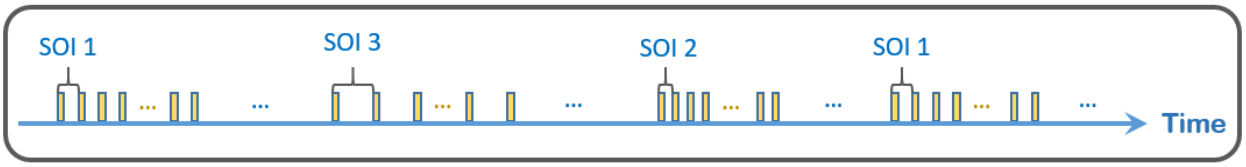

Figure 1. 4 Illustration of regular-SOI paradigm

The whole stimulation consists of a set of individual blocks of repetitive stimuli being separated by long silence. Repetitions of pure tones are presented within each block with a certain SOI. The SOI is systematically varied across blocks.

The regular-SOI paradigm is well suited for characterizing the kinetics of adaptation in a steady state, and thus, the temporal characteristics of adaptation. Response amplitudes recover along an exponential saturation curve as a function of SOIs across a wide range. Therefore, stationary adaptation in the steady state can be characterized by a single time constant τ obtained by exponential fitting (Lü et al., 1992; Lu et al., 1992).

1.4 Motivation and objectives of the study

1.4.1 Research questions and hypothesis

Auditory adaptation is processed by multiple mechanisms within the hierarchical auditory network, at various levels of auditory processing, in an interactive manner. The AC thereby seems to play a role in the network dynamics of adaptation by intracortically shaping adaptation and/or by corticoefferent modulation of subcortical adaptation processes. This raises the yet unresolved question how the AC, or more specifically, how the layer-specific inputs and outputs to the cortex, and the intracortical circuit interactions across layers transforming the input into the output, contribute to adaptation. To address this question, my goal was to disentangle cortical input from intracortical processes in the primary auditory cortex (A1), and to estimate and quantify the contribution of the intracortical circuitry to adaptation in a layer specific

resolution. To achieve this goal, I combined two approaches, the layer-specific quantification of synaptic mass activity by current-source density analysis (Happel et al., 2010; Szymanski et al., 2009) with the pharmacological silencing of the A1 activity by $GABA_A$-receptor agonist muscimol (Bäuerle et al., 2011; Happel et al., 2010). Such a combined approach has been previously used to characterize the origin of the frequency tuning of auditory cortical responses (Liu et al., 2007).

The main hypothesis of this work is that, if cortical adaptation relied on differences in adaptation of the lemniscal and non-lemniscal input streams to the A1, layer-specific differences in adaptation described in the literature should already be apparent at the stage of initial, afferent inputs to granular and infragranular layers of A1. After silencing intracortical transmission, adaptation inherited from subcortical input should remain unchanged in its properties. Furthermore, if the cortical circuitry contributes to cortical adaptation, there should be a difference observable in the intracortical processing across layers, and cortical silencing should lead to layer specific changes in adaptation.

1.4.2 Methodological approaches to achieve these objectives

To tackle these questions, cortical columnar circuit activation needs to be measured at a high spatiotemporal resolution simultaneously across layers. Hence, I recorded laminar profiles of LFPs at high spatial resolution in A1 of anesthetized Mongolian gerbils (*Meriones unguiculatus*). The LFP measures extracellular potentials and covers a special scale of around 1 mm (Table 1, Nelken & Ulanovsky, 2007,) corresponding to a neuron population between 1000 and 100,000 (Buzsáki et al., 2012). Multi-channel electrophysiological recordings therefore provide detailed LFP current gradient information across all the cortical layers. In order to obtain a measure of neural responses that is more directly related to synaptic currents, I calculated current source density distributions from the LFP-profiles across layers. Using current source density (CSD) analysis, which will be further explained in section 2.4.1 (Mitzdorf, 1985), I reconstructed the layer-specific sink and source components that generate the current gradient that the LFP captures. In order to disentangle the intracortical from the thalamocortical contribution to the cortical RS, the intracortical activity was silenced by the $GABA_A$ agonist muscimol. As for stimulation paradigm, I used the regular-SOI paradigm, as it specifically characterizes response suppression as a fundamental aspect of adaptation. This enabled me to

quantify both, the strength and the temporal characteristics of adaption as a stationary system property.

2. Materials and Methods

All experiments were carried out with healthy and adult male Mongolian gerbils (*Meriones unguiculatus*, 3 - 6 months of age, 70-90 g bodyweight, n = 10). The experiments were conducted in accordance with ethical animal research standards defined by the German Law and approved by the ethics committee of the state of Saxony-Anhalt under the license 42502-2-1394LIN. The experimental and the terminal procedures after the acute recordings were all in accordance with the principles and regulations as described by Grundy (2015) in *The Journal of Physiology*.

Animals were subject to and kept under anesthesia since surgery and during the whole measurement procedure. Electrophysiological recordings comprised two experimental paradigms, 1) the presentation of a series of pseudo-randomized pure tones with different frequencies to determine the frequency response at the recording site, and 2) the presentation of various sequences of pure tones with identical frequencies and regular stimulus onset intervals that differ between sequences (regular-SOI paradigm) to determine RS of the cortical response. Both paradigms were performed in an untreated and a treated (cortical silencing with muscimol) state. At the end of the experiment, animals were sacrificed with minimum suffering to avoid an overly painful recovery. A guillotine was used after the injection of an overdose of anesthetic infusion. The carcasses were disposed after the death of the animal has been confirmed.

2.1 Mongolian gerbil as an animal model for auditory research

To understand mechanisms underlying auditory processing, it is crucial to gain knowledge of the anatomy and the functional organization of the auditory system. In order to overcome certain limitations in the experimental approaches in human subject, e.g. severe ethical regulations regarding the applicability of recording techniques and drug manipulations as well as the low availability of subjects with lesions, extensive studies have been carried out on animal models. During recent decades, the small rodent Mongolian gerbil (Figure 2.1) has become a

frequently used mammalian model in auditory neuroscience. The foremost reasons for the growing research interest in using Mongolian gerbils in hearing research are as follows:

Figure 2. 1 A photo of Mongolian gerbil (*Courtesy of Fahmida Akter*)

1) Similar to humans, the auditory system of gerbils has a high sensitivity at low frequencies in the range between 0.1 and 16 kHz, which are critical for speech perception in humans and the perception of animal sounds in gerbils (Otto & Jrge, 2012; Ryan, 1976), whereas for rats and mice, the response thresholds are much higher in comparison to gerbils for audio frequencies below 4 kHz (see Figure 1 of Otto & Jrge, 2012). Therefore, gerbils are better suited to study neural processing in frequency ranges relevant for human audition than rats or mice.

2) Gerbils perform well in various auditory learning paradigms (Ohl et al., 1999; Sarro & Sanes, 2010; Wrobel et al., 2018; Zempeltzi et al., 2020) (Ohl et al., 1999; Wetzel et al., 1998; Zempeltzi et al., 2020).

3) Knowledge about the functional anatomy of the cortical and subcortical system is well established in the gerbil (Budinger et al., 2000; Deane et al., 2020; Happel et al., 2010; Saldeitis et al., 2014; Scheich et al., 2007a). My research thereby strongly benefits from immediate and strong in-house expertise in the research field.

4) The enlarged middle ear cavities of gerbils allow easy access to the cochlea turns (Thomas et al., 1993).

5) Gerbils are relatively small and easy to breed and keep under laboratory conditions. Also, they rarely show complications or inflammatory responses with surgical interventions.

In conclusion, the gerbil is an ideal animal model for gaining further understanding of the

cortical processing of the auditory adaptation.

2.2 Electrophysiological recordings and pharmacological intervention

2.2.1 Surgical procedure – exposure of auditory cortex and implantation of electrode

The surgical preparation of the subject and the electrophysiological recordings were performed according to the procedure laid out in Brunk et al., 2019; Happel et al., 2010; Ohl et al., 1999. Anesthesia was induced before the surgery by an intraperitoneal injection of an infusion of 45% v/v ketamine (50 mg/ml, Ratiopharm GmbH), 5% v/v xylazine (Rompun 2%, Bayer Vital GmbH), and 50% v/v of isotonic sodium-chloride solution (154 mmol/l, B. Braun AG) with an initial dose of 0.004 ml/g bodyweight. Later on, the anesthetic status was maintained by the same ketamine/xylazine infusion at a rate of 15 mg/kg·h. The anesthetic status was checked on a regular basis every 10-25 min via the withdrawal-reflex of the hind paw and by the observation of the breathing rate. The body temperature was kept stable at 34°C with a controlled heating pad.

Resection of the scalp and the right temporal muscle was performed to expose the nasal, frontal, parietal and right temporal bones. Head fixation for the electrophysiological recordings was achieved by attaching an aluminum bar onto the exposed nasal bone plate (Figure 2.2A) with UV-curing glue (Plurabond ONE-SE and Plurafill flow, Pluradent). Insulation was stripped off about 1 mm from the tip of a Teflon-coated stainless-steel wire (Ø = 200 µm), and the bare end was formed to a loop. The loop was implanted through a small hole (Ø = 1 mm) drilled in the left parietal bone (Figure 2.2A) with a good contact to the dura mater, which served as a reference electrode for the recordings. The reference wire was glued onto the skull for a stable fixation. Finally, the right AC area was exposed via a trepanation of about 4 mm in diameter. At the end of the surgery, the animal received a subcutaneous injection of an infusion of 0.03 ml Robinul (0.2 mg/ml) and 0.1 ml 5% Glucose. This injection helps to ease breathing as the anesthesia might block the cardiac vagal inhibitory reflexes. It also ensures energy supply during the hours of recordings.

In preparation for the electrophysiological recordings, the animal was brought to the recording chamber, a Faraday-shielded soundproof acoustic room, right after the surgical preparation. The head of the animal was fixed to a head holder via an aluminum bar. Then, a

small incision was made into the dura with a slightly hooked needle above the identified implantation site in A1. Afterwards, a 32-channel shaft electrode (NeuroNexus A1x32-50-413) was implanted into A1 perpendicular to the cortical surface (Happel et al., 2010). The recording position in the A1 was chosen based on vascular landmarks at the surface of the exposed cortex as described in literature (Figure 2.2B, c.f. Ohl et al., 2000; Scheich et al., 2007; Happel et al., 2010). The 32 recording channels were equally distributed along the electrode shaft tip with a channel spacing of 50 µm, which in total covers a recording range of 1600 µm that ensures the observation radially through the whole neocortex.

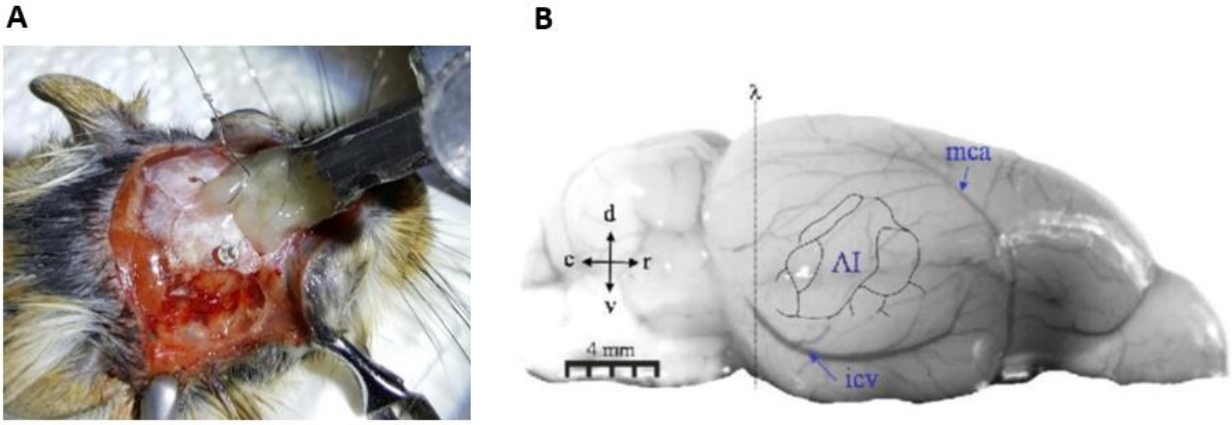

Figure 2. 2 Surgical preparation of exposure of the AC

A. Head fixation, implantation of the reference electrode and exposure of AC. **B. Lateral view of the gerbil brain** (Ohl et al., 2000; Scheich et al., 2007). Typical positioning of the electrode array at the A1 is indicated in relation to the rostro caudal position of the anatomic landmark λ and the characteristic vascularization pattern formed by the ascending branches of the inferior cerebral vein (icv) and the descending branches of the middle cerebral artery (mca). The A1 is typically located between icv and mca. –- Indexes of anatomical terms of location: c-caudal, d-dorsal, r-rostral, and v- ventral.

2.2.2 Acute electrophysiological recordings

The recording setup is sketched in Figure 2.3. Audio stimulation was generated with Matlab (Mathworks, R2006b), converted into an analog signal (sampling frequency 10 kHz, NI PCI-BNC2110, National Instruments), routed through an attenuator (gPAH, Guger Technologies), and amplified (Thomas Tech Amp75). Finally, the sound was presented (transmitted) by a loud speaker (Tannoy arena satellite KI-8710-32) located 100 cm behind the animal. A microphone and conditioning amplifier were used to calibrate the acoustic stimuli (G.R.A.S. 26AM and B&K Nexus 2690-A, Bruel & Kjær, Germany).

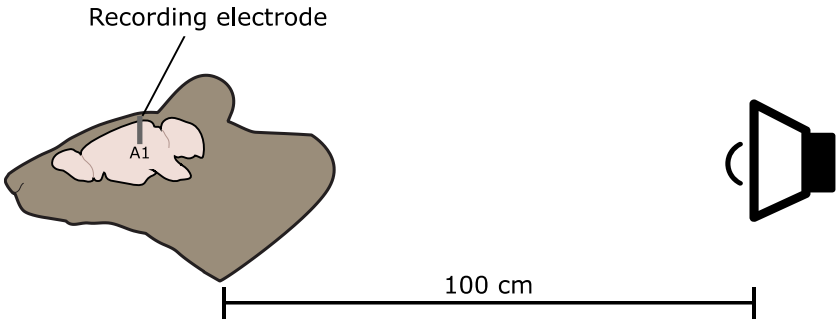

Figure 2. 3 Schematic for acute measurements during auditory stimulation

A multi-channel electrode was implanted into the A1 of the anesthetized gerbil. Pure tones were presented by a loud speaker from 100 cm distance behind the animal (*Figure modified from https://scidraw.io by Artist Ann Kennedy*).

Brain signals were fed via an Omnetics connector to a head stage (HST/32V-G2O LN 5V, 20x gain, PlexonInc), and then via a cable to a PBX2 preamplifier (Plexon Inc.), which band-pass filtered (0.7-300 Hz) and further amplified the signals 500-fold. Due to the high-frequency cut-off of the filter at 300 Hz, fast spiking activity was reduced, and the recorded signals reflected mainly slow synaptic activity. The recorded analog signals were then digitized at a sampling frequency of 1 kHz with the Multichannel Acquisition Processor (Plexon Inc.) and stored offline for further analysis.

2.2.3 Pharmacological silencing of corticocortically relayed processing

In order to separate the thalamocortical and intracortical synaptic contributions to the evoked cortical response, the intracortical activity was silenced by the $GABA_A$ agonist muscimol. A dose of 20 µl muscimol (8.23 mM muscimol, TOCRIS bioscience, batch no: 9C/107090) was dissolved in isotonic sodium-chloride solution and applied topically onto the cortical surface (Happel et al., 2010). This concentration and volume have been reported to be appropriate to effectively silence all the cortical layers, but to not affect the subcortical activities (Edeline et al., 2002; Happel et al., 2010). Diffusion of muscimol through cortical layers was monitored by recording cortical responses to tones of different frequencies. After about one hour, only residual thalamocortical inputs could be detected by the early current sink activation in granular layers III/IV and in infragranular layer Vb. The recovery of the intracortical processing has been

reported to take more than 10 hours after muscimol application (Happel et al., 2010), which guarantees sufficient time for the RS recordings at a stabilized silenced state.

2.3 Experimental design and auditory stimulation paradigms

2.3.1 Design overview

The overall experimental design is shown in Figure 2.4. Right after electrode insertion, the frequency response (FR) was measured in order to evaluate the status of the cortical response *(Untreated FR*). It took typically about 1 h, until a stabilized cortical response was observed (Deane et al., 2020). Once the response has stabilized, the best frequency (BF, see section 2.3.2) and non-best frequency (non-BF) were determined. In the following RS measurement, which lasted about 4 h (ca. 25 min/session × 8 sessions) and is labeled as *Untreated RS* condition, the regular-SOI paradigm was presented to investigate the dependence of the balancing between the suppression and recovery process on the SOI, for both BF and non-BF stimulation. After this measurement has been completed, the $GABA_A$ agonist muscimol was applied onto the surface of the A1. Immediately afterwards, another set of FR measurement was carried out for an hour during which the status of cortical silencing was monitored (*Muscimol FR*). After successful cortical silencing, a further set of RS measurements (*Muscimol RS*) was carried out for about 2 h (ca. 25 min/session × 4 sessions), with only BF being presented. The decision of abstaining from the non-BF recordings was based on the fact that the cortical silencing resulted in very weak non-BF evoked responses, and, as a consequence, in a rather low signal-to-noise ratio.

Figure 2. 4 Design overview

Within the first hour after electrode implantation, the FR responses were tested while monitoring the gradual stabilization of responses (*Untreated FR*). Once the response has stabilized, the BF was determined for the recording site. During the *Untreated RS* measurements, the regular-SOI paradigm was presented with both BF and non-BF stimuli. After the application of muscimol, FR responses were measured for another hour (*Muscimol FR*), during which the status of cortical silencing was monitored until the muscimol had passed through all cortical layers. After cortical silencing, RS was measured at BF only (*Muscimol RS*).

2.3.2 Frequency response measurements

In FR measurements, series of pseudo-randomized pure tones (seven audio frequencies covering the range from 0.25 to 16 kHz in octave steps, tone duration 200 ms including linear rise- and fall times of 5 ms each, randomized SOIs of 800- 1000 ms, sound pressure level 65 dB, 50 tone repetitions for each frequency), while electrophysiological recordings of the cortical response were performed. Each session of FR measurement lasted about 7 min, and immediately after each session, the next session was started. During the recordings, the LFPs were transformed into CSD profiles and being examined. The stabilized response level was characterized by steady activity of the sinks and by an identical frequency response pattern across several consecutive sessions. After the response has stabilized, the BF was defined as the frequency evoking the largest root-mean-squared (RMS) amplitude of the CSD in granular layers in the time window between 15 ms and 64 ms after tone onset. This selected time window typically covers the activation of the early sinks. The audio frequency of the non-BF stimulus was defined as the frequency two octaves away from the granular BF. The choice of non-BF of either two octaves above or below BF depended on which of them had a clearer contrasting response strength against BF. The individual BF and non-BF values for each subject obtained with this procedure are listed in Table A.2.1.

2.3.3 Repetition suppression measurements

To investigate the SOI-dependence of the balanced state between RS and recovery, a modified regular-SOI paradigm was applied. *Untreated RS* and *Muscimol RS* conditions consisted of 8 and 4 recording sessions, respectively, and each session lasted about 25 min. This session design guarantees sufficient data and also enables regular checks of the anesthesia state between the sessions. The presented stimulation for each recording session (as shown in Figure 2.5) included 60 trials that shared a similar structure, i.e. each trial started with a sequence of stimuli followed by a silent interval, which in turn preceded the tone sequence of the next trial. Within each trial, a sequence of pure tones (100 ms tone duration including linear rise- and fall times of 5 ms each, 65 dB SPL) was presented with a constant SOI that was pseudo-randomly selected from a list of ten SOIs (0.219, 0.328, 0.438, 0.656, 0.875, 1.313, 1.750, 2.626, 3.500, and 7.000 s). Further, within each trial, the frequency of the tones was either BF or non-BF for the *Untreated RS* condition (with the order of presentation of BF and non-BF series being

randomized), and only BF for *Muscimol RS*. As a trade-off between minimizing recording time and maximizing the number of tone repetitions, a tone-sequence duration of 7.2 s was chosen for SOIs < 2.626 s, and of 14.2 s for SOIs ≥ 2.626 s. Each trial type was defined by a combination of a distinct tone frequency (BF or non-BF) and a given SOI, and was repeated 24 times. The total amount of 480 trials for *Untreated RS* (2 tone frequencies × 10 SOIs × 24 trial type repetitions) were equally distributed over eight recording sessions (60 trials/session), and the 240 trials for *Muscimol RS* were equally spread over four sessions (1 tone frequency × 10 SOIs × 24 trial type repetitions). Details on the tone-sequence duration as well as the number of tone repetitions for each SOI are listed in Table A.2.2. The silent interval between the last tone of the preceding and the first tone of the consecutive tone sequence was the same for all trials and lasted 14 s to allow sufficient recovery time for the system.

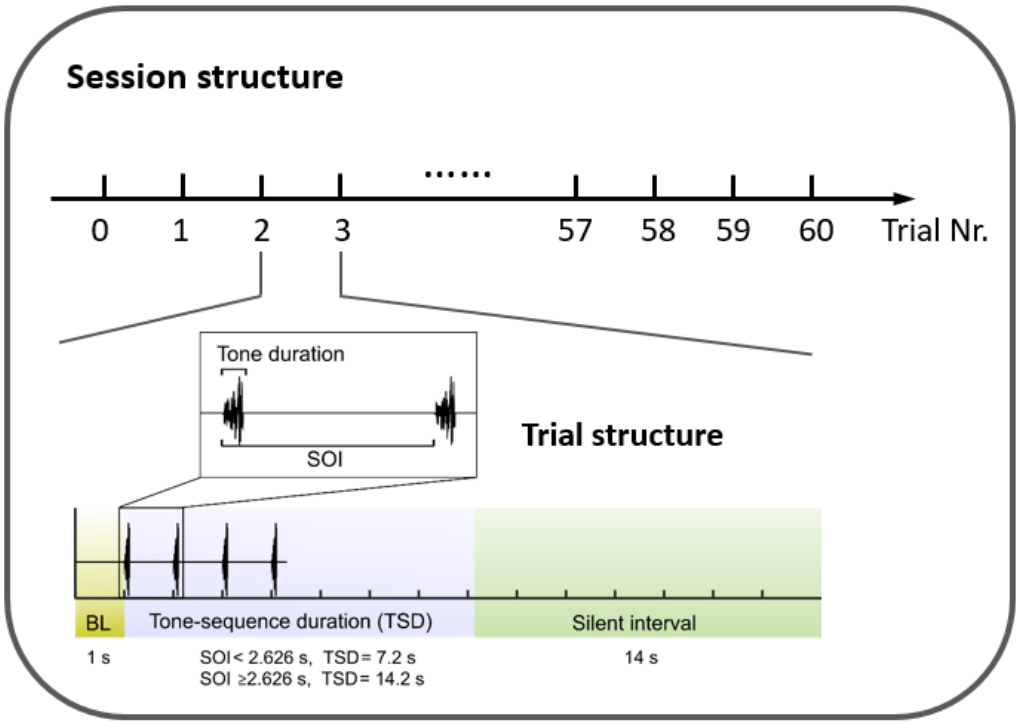

Figure 2. 5 Structure of recording session

The *upper panel* illustrates a RS measurement session, which contains 60 sequential trials that share a similar trial structure. The *lower panel* presents the structure of a single trial. The trial starts with a sequence of repetitive tones that are separated by a fixed SOI. Depending on the SOI value, the tone-sequence duration is either 7.2 s for SOIs smaller than 2.626 s or 14.2 s for the rest SOIs. When the tone-sequence ends, a 14 s silent interval follows. The trial ends at the end of the silent interval and right after, the next trial starts. During data analysis, the last second of a silent interval of the preceding trial was taken as the baseline of the current trial.

2.4 Data analysis

2.4.1 Data pre-processing and current source density analysis

The raw plexon data files were first converted into Matlab files via custom-written scripts (Mathworks, R2011a). Next, the channels were sorted according to their recording depth. Channel interpolation was applied to channels that were either damaged or did not show an acceptable recording quality. Two experienced observers inspected all channels independently. Only channels consistently identified by both observers were interpolated. Data from one of the ten subjects was excluded during data analysis due to its unusually weak cortical response, potentially caused by cerebrovascular damage during surgery or by the dura incision.

Based on the recorded LFPs, the current source density (CSD) was computed, which is the second spatial derivative of the field potential Φ to the spatial coordinate z perpendicular to the laminae (Mitzdorf, 1985), using Matlab (Mathworks, R2011a):

$$-\mathrm{CSD} \approx \frac{\delta^2\Phi(z)}{\delta z^2} = \frac{\Phi(z+n\Delta z) - 2\Phi(z) + \Phi(z-n\Delta z)}{(n\Delta z)^2}, \qquad (1)$$

with the spatial sampling interval Δz and the differential grid n. Prior to CSD calculation, LFPs were spatially smoothed using a weighted Hamming window of seven channels corresponding to a kernel size of 300 µm (Happel et al., 2010).

The CSD distribution reflects the spatiotemporal transmembrane current flow. Current sinks are indicative of currents flowing from extra- to intracellular space, while current sources mainly reflect the capacitive return currents across the membrane that counterbalance the local sink activity in neighboring layers. Figure 3.1A and 3.1B show examples of CSD profiles evoked with tones at BF in the *Untreated FR* and the *Muscimol FR* conditions. Based on the location of the early sinks and sources, the different cortical layers are marked by the black dashed lines.

2.4.2 Characterizing layer-specific CSD-responses

For the FR data, tone-evoked laminar LFP epochs were extracted at a time window between

-40 ms and 160 ms relative to tone onset, and then averaged across tone repetitions (n = 50), separately for each tone frequency (n = 7) and animal (n = 9). Then, the LFP profile was transformed into the CSD profile based on Equation 1 (Figure 2.6A, CSD value of each spatiotemporal point was color coded). To determine granular and infragranular responses to the initial thalamocortical input, layer-specific CSD response traces were extracted from averages across channels covering the initial sinks in granular layer IV and the infragranular layer Vb, respectively (Figure 2.6B). Channels that could be assigned to one of the two sinks were identified for each animal by two independent observers. Only channels consistently identified by both observers were included in the analysis.

For the RS measurements, single trial LFPs (displayed in the left panel of Figure 2.6A) were first averaged across trials (n = 24 for each trial type, see Sect. 2.3.3), and then transformed into CSD profiles (right panel of Figure 2.6A), separately for each condition, SOI (n = 10), and animal (n = 9). To obtain well adapted tone responses reflecting steady state RS, averaging was only performed using those responses to tones that occurred 2 s after the onset of the sequence (this means 2 to 24 tone repetitions, depending on the particular SOI value and the overall sequence duration, see Figure 2.5 and Table A.2.2). The granular and infragranular response traces were computed in the same way as described above for the FR data.

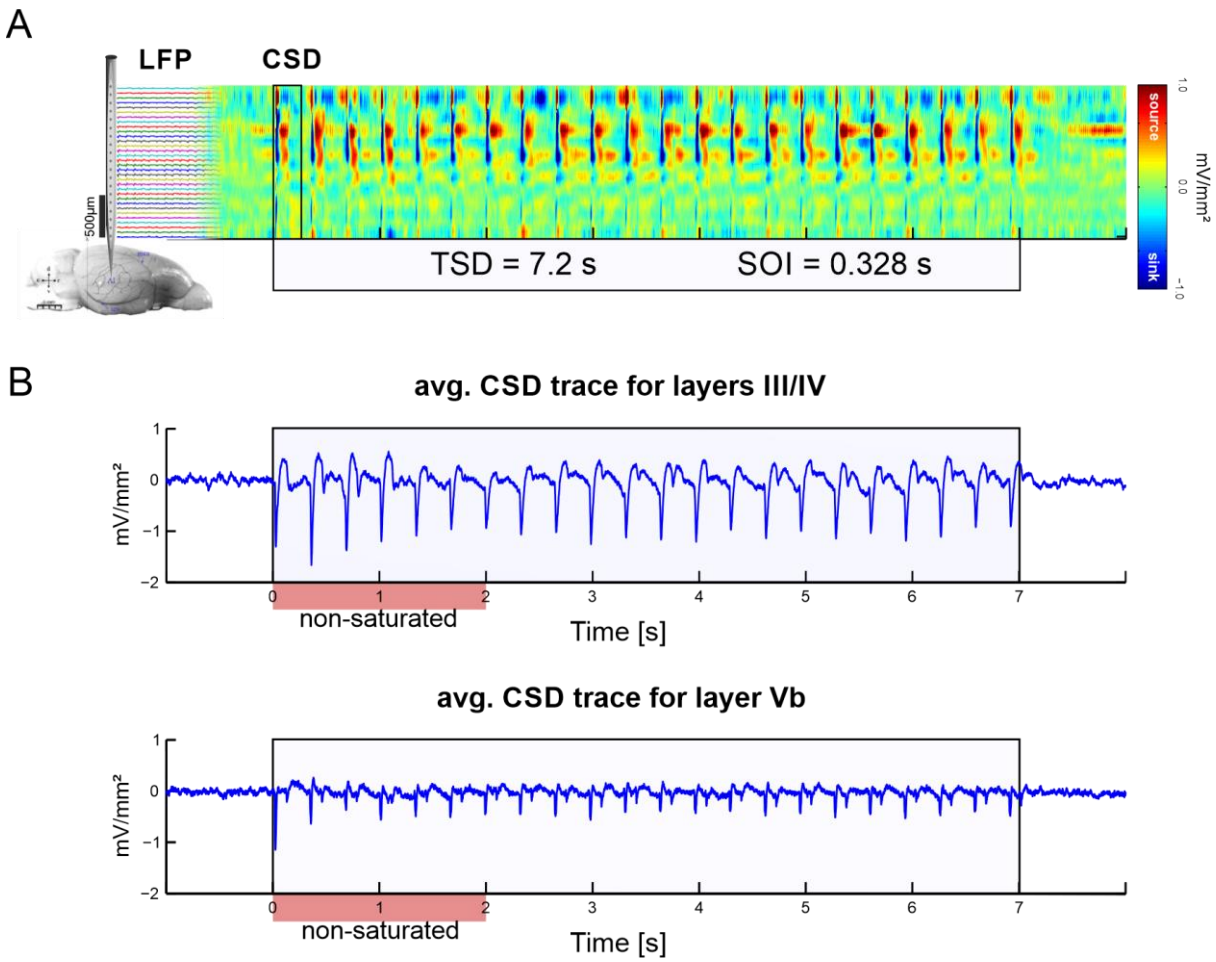

Figure 2. 6 CSD profile and layer specific CSD traces in response to a tone sequence (single subject)

A. The averaged LFPs in response to BF tone sequences with SOI of 0.328 s were transformed into CSD profile, with CSD values being color coded according to the color bar at the right side of the panel. **B.** Granular (*upper panel*) and infragranular (*lower panel*) CSD traces evoked by BF-tone sequences and averaged across channels covering each sink showed different peak magnitudes. Note that the tone-evoked response decreased across tone repetitions roughly within the first 2 s, as indicated by the red color bar along the abscissa.

During further analysis of both FR and RS data, the following response measures for each SOI, condition, and subject were applied. First, I extracted the amplitude and the latency of the peak of the CSD trace, which will be respectively referred to as sink amplitude and sink latency in the following text. The peak of the sink is an important response measure, which reflects the maximum instantaneous inflow of excitatory synaptic mass current during the sink activation in response to a tone. The peaks were always localized within the first 50 ms after tone onset. Second, the sink integral was determined, which reflects the overall transmembrane current flow during sink activation. I calculated the cumulative sum of the layer-specific CSD response traces within the first 100 ms after tone onset. The cumulative sum is the result of the summation of the response as it changes with time and approximates the integral of a response trace in a given time window. For a single (monopolar) negative trace (such as a sink response),

for example, the cumulative sum converges to its minimum value at a distinct point in time, thus reflecting the amount of the overall synaptic mass current flow into the intracellular space during sink activation, respectively. The peak amplitude of the sink integral is termed as peak integral, here.

2.4.3 Characterizing the balancing kinetics between RS and recovery

When a tone sequence was presented with a certain SOI, the tone-evoked response strength decayed within about the first 2 s until it reached a fairly stabilized level, as shown exemplarily in Figure 2.6B. The speed of this decay and the stabilized response strength depend on the SOI value. This stable level can be seen as a steady state during with the suppression and recovery processes reached a balance, as both of the suppression and recovery are impacted by the SOI value. To characterize the kinetics of RS at the steady state, an exponential function (2) (based on Lu et al., 1992; Zacharias et al., 2012) was fitted to the sink amplitudes of the early granular and infragranular sink as a function of SOI, as well as for the peak integral according to:

$$y(SOI) = A\left[1 - \exp\left(-\frac{SOI - t_0}{\tau}\right)\right] \qquad (2)$$

with saturation amplitude A, the intersection t_0 of the exponential curve and the abscissa, and the time constant τ quantifying the lifetime of the balance between the SOI dependent suppression and the recovery from RS. For the actual fitting process, the initial parameter for A was set to the maximum response across all SOIs, which is typically at SOI value of 7 s, and for τ it was set to 0.3s. In case the fitting failed with these initial settings, the initial value for τ was set to 0, which always yielded valid fits. Setting τ at 0 was because the failed fitting are mostly due to a very steep therefore not exponential curve, which can be seen as no appearance of significant suppression t. The parameter t_0 was fixed to 0.1 s, i.e. the value of the stimulus duration, where individual tones merge into a continuous tone without gap, and no onset response should be triggered. The iterative least squares approach (nlinfit function, MATLAB R2011a), a regression analysis method to approximate fitting in overdetermined systems by mitigating outlier influence, was used to achieve a final estimate of the remaining two free parameters, A and τ. Other initial values and fitting options were also explored, including t_0 being a free parameter, and an approximation of the starting value of τ based on the data. None

of these approaches changed the results substantially, but rather increased the confidence intervals. In the end, fixing t_0 to 0 s and a starting τ value of 0.3 s was the most parsimonious and robust fitting option.

To quantify the strength of RS at each individual SOI, the repetition suppression index (RSI) was computed for both the sink amplitude and the peak integral-values by adapting the equation describing the SSA index (SI) as initially suggested by Ulanovsky et al. (2004):

$$\mathrm{RSI}_{\mathrm{SOI}} = (a_{\mathrm{SOI}} - A)/(a_{\mathrm{SOI}} + A) \qquad (3)$$

Here, a_{SOI} is the stabilized response strength at each SOI, measured either by the sink amplitude or peak integral. A is the saturated sink amplitude or the peak integral estimated via exponential fitting (Equation 2), respectively. The saturation level approximates the response strength for infinite SOI, i.e. the response that is unaffected by preceding tone stimulation thus without yet RS. The RSI measure allows a comparison of the RS strength at each SOI, irrespective of the overall response strength, or the type of response measure.

2.4.4 Correlation analysis of CSD responses and different RS kinetics

My analysis revealed two different RS kinetics of the granular and the infragranular sink amplitude (see Results). A short-lived granular kinetics was found with time constants at around 0.2 s, and a long-lived infragranular kinetics with time constants around 0.5 s. To investigate the kinetics governing the cortical response at other latencies and in other layers, I carried out a correlation analysis which determined whether the CSD response at a certain latency and depth is stronger correlated with the short- or the long-lived kinetics. In particular, for each point in the CSD profile determined by time and depth, I first calculated a correlation coefficient between the CSD values and the exponential SOI function fitted to the granular/ infragranular sink amplitude across SOIs, respectively. To correct for latency shifts of the responses across SOIs, CSD response profiles were aligned to the peak latency of the initial infragranular sink, and results are displayed in a time window from-50 to 100 ms relative to the peak latency of the early sink. I then determined, whether CSD values at a latency and depth were stronger correlated with the short-lived ($\tau_{\mathrm{gran}} \cong 0.2$, BF stimulation under untreated condition) or the long-lived ($\tau_{\mathrm{infra}} \cong 0.5$ s) kinetics as a function of SOI. Non-significant correlations ($p < 0.05$)

were set to 0. For convenient comparison, the positive correlation was set between the peak sink amplitudes and the negative sink CSD-values, which is the research focus here, whereas the negative correlations with the sink amplitudes as well as the positive source CSD-values were set to 0. Then I calculated Fisher-z-values of the two correlation coefficients for each latency and depth, and then the t-value difference between them. A positive t-value indicated that the CSD correlated stronger with the short-lived granular kinetics, and a negative t-value that it correlated stronger with the long-lived infragranular kinetics.

Differences between fast and slow kinetics correlation were statistically evaluated by performing a permutation test on the t-values. Correlation t-values of both fast and slow kinetics were randomly permuted for 1000 times, for each condition and each subject. To avoid repetitive testing a single permutation sample, only the 2.5% and the 97.5% percentile of permutation samples of the t-values were selected (Groppe et al., 2011). For each spatiotemporal point in the CSD profile, when the t-value was smaller than the 2.5% percentile of the random distribution of the permutation samples, the correlation with the slow kinetic was considered to be significantly higher than the correlation with the fast kinetic. Conversely, when the t-value exceeded the 97.5% percentile, then the correlation with fast kinetic is considered to be significantly higher.

2.4.5 Statistical analysis using bootstrapping

Although the sample size, i.e. the number of subjects that entered the analysis of the experiments described in this work (n = 9), is rather typical for this kind of electrophysiological recordings, this relatively small number nevertheless has a limited power for drawing general conclusions on a group level. On the level of the single subjecs, the bootstrap method enabled the generation of surrogate data, and, thus, increased the sample size of experimentally recorded data significantly. Bootstrapping can provide an approximation of the true distribution with sufficient resolution (Efron, 1979). Bootstrapping enables the strengthening of statistical power, especially for data sets originally consisting of a small number of samples, for which the determination of robust means and convincing confidence intervals (CIs) is subject to large uncertainties. Applied to the experiments described here, the bootstrapping method allows, in particular, the determination of robust median values and CIs of the response measures and the exponential fitting parameters. This should also reduce variability across subjects, and

improve power on the group level.

In the conventional sense, non-parametric bootstrap describes the random sampling of data with replacement, although several different variants such as random sampling without replacement or parametric bootstrapping do exist. An important assumption for the application of the bootstrapping method is that the data should be considered as independent and identically distributed (IID) In particular, concerning the validity of the IID assumption for the present RS data set, two different cases need to be considered: the independence of the series of tones between consecutive trials (which are separated by the silent interval of 14 s), and the independence of individual tones separated by the constant SOI within a trial. Since the 14-s interval between two subsequent tone-sequences allows almost full recovery from synaptic suppression, each single trial CSD trace can be considered to fulfil this condition. Notably, this also holds for the single tone responses, assuming that—following the classical signal-plus-noise model for trial averaging—the trial-to-trial response consists of a deterministic part (the signal) and a part that varies from trial to trial (the noise). Provided the response can be considered as deterministic, at least in the time interval about 2 s after trial onset, when the response is stabilized, the IID assumptions are met and the application of bootstrap is possible.

The application of the bootstrap technique is illustrated here for the RS experiment. For each trial type of the present data, i.e. for each combination of tone frequency (BF or non-BF) and SOI, there were 24 individual trials (response traces to tone sequences) available, which constituted the data set on which the bootstrap analysis was based. For each tone frequency and SOI, bootstrap was performed by randomly drawing with replacement combinations of 24 CSD traces out of the 24 original trials, and the mean has been calculated for each sample set. This procedure (sampling with replacement) was performed 1000 times (999 repetitions plus the original sample set), separately for each trial type, layer, condition (untreated or muscimol condition), and subject, to derive for features such as peak amplitude and peak latency of both the sink activity and the sink integral. Out of these 1000 mean traces, the median trace and the 95% CI were deduced for each animal.

For group level analysis, I used the median values of the different response measures and fitting parameters obtained via the bootstrapping as robust estimates for single animals. For statistical testing for differences in time constants and saturation amplitudes between conditions (layer, BR/nonBF, treatment) on a group level within subjects, I employed Friedman

tests, which is a non-parametric version of a one-way repeated measures ANOVA.

3. Results

The goal of this research is to investigate the role of intracortical microcircuits in processing cortical adaptation with layer-specific resolution in the A1 of anesthetized Mongolian gerbils. Observation of laminar synaptic mass activity was achieved by carrying out CSD analysis of the cortical responses. In order to disentangle thalamocortical from recurrent intracortical input, the $GABA_A$ agonist muscimol was applied topically onto the exposed A1 surface to silence the intracortical processing. For the cortical responses, steady states of RS at a range of SOIs were studied using the regular-SOI paradigm. The temporal characteristics the SOI-dependent RS were characterized by estimating the time constant τ for granular and infragranular layers.

3.1 Determination of cortical responses

In order to determine the CSD response evoked by pure tones as well as the FR function, offline analysis of FR data was carried out as described in Section 2.4.2. The CSD analysis reconstructed the current sink and source activities that generated the voltage gradients recorded as LFP traces; therefore, it is more directly related to the synaptic mass activity than LFPs. BF tone evoked CSD profiles are shown in Figure 3.1A and 3.1B respectively for *Untreated FR* and *Muscimol FR* recordings. Distinguishing and prominent sink activities appear in granular layer IV at a cortical depth of about 250 to 500 µm and in the infragranular layer Vb at about 900 to 1200 µm, both starting at around 20 ms after tone onset (Figure 3.1A). After cortical silencing, residuals of the initial granular and infragranular sinks due to thalamocortical afferent input were still visible, but, in general, the sink and source activations were much weaker and had a shorter duration compared to *Untreated FR*.

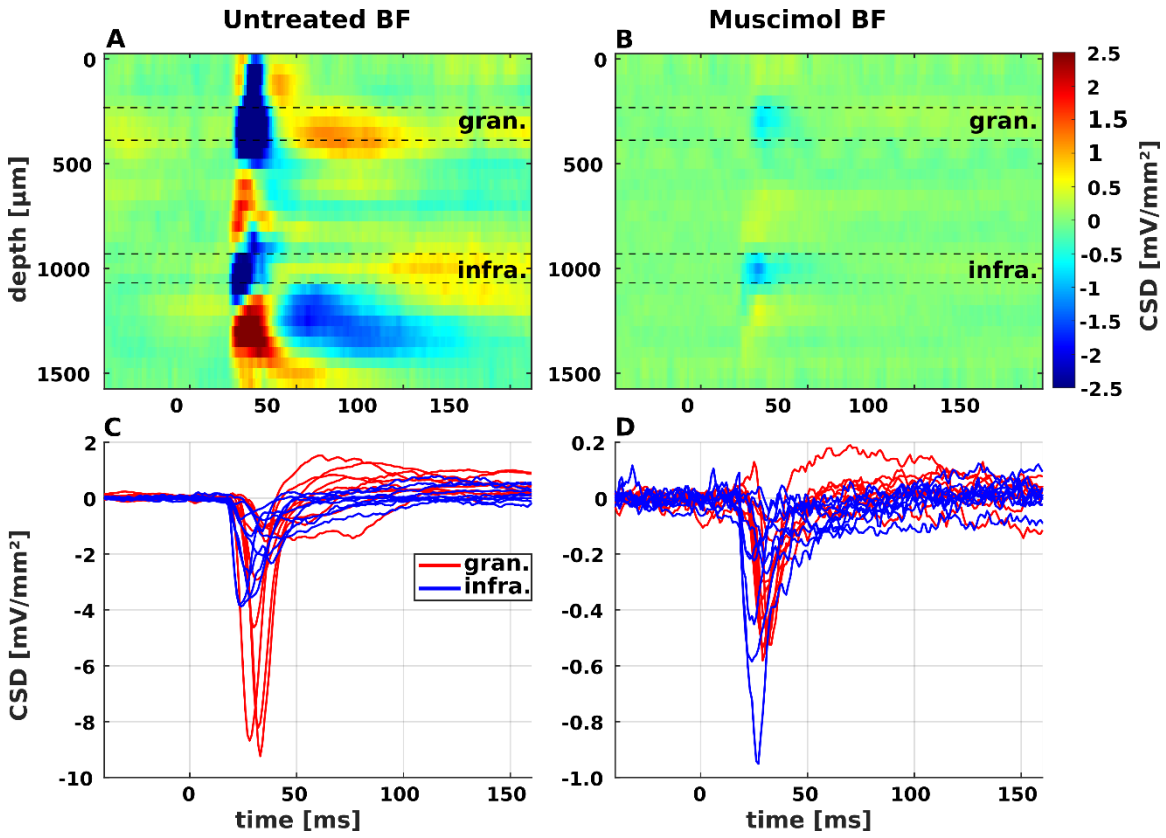

Figure 3. 1 BF-tone evoked CSD profiles (*single subject*) and layer-specific CSD traces (*from all subjects*)

In the upper two panels, BF-evoked CSD profiles are displayed for the *Untreated FR* (**A**) and the *Muscimol FR* recordings (**B**). Current sinks indicating depolarizing currents are shown in blue, and current sources (hyperpolarizing currents) which balance the sinks are shown in red and yellow, whereas zero net currents are plotted in green (see color bar). Based on the location of the early sinks and sources, the different cortical layers (roman numbers) were marked by the black dotted lines. The lower two panels show the CSD traces of granular (red) and infragranular (blue) layers of all animals (n = 9) recorded at BF during the *Untreated FR* (**C**) and the M*uscimol FR* (**D**) recording. Note that the scales of the ordinates of the two panels differ by one order of magnitude.

Figures 3.1C and 3.1D show the individual subject's CSD traces of the granular and infragranular sinks obtained at the granular BF for the *Untreated FR* and the *Muscimol FR* recordings, respectively. Granular and infragranular sink activities are reflected by initial negative peaks, which dominate the overall responses to the tone. The peak latency occurs between 20 and 40 ms and varies across subjects in both layers. In the *Untreated FR* recording, granular sinks tend to be larger in amplitude than infragranular sinks (in 7 out of 9 animals), and also had longer response durations. In the *Muscimol FR* recording, the peak amplitudes of the sink activity of both the granular and infragranular sinks were by about an order of magnitude smaller compared to the *Untreated FR* recording, due to the cortical silencing. Moreover, the response strengths reflected by the peak amplitude varied less between the granular and infragranular sinks, while the variation of peak latency across subjects remained.

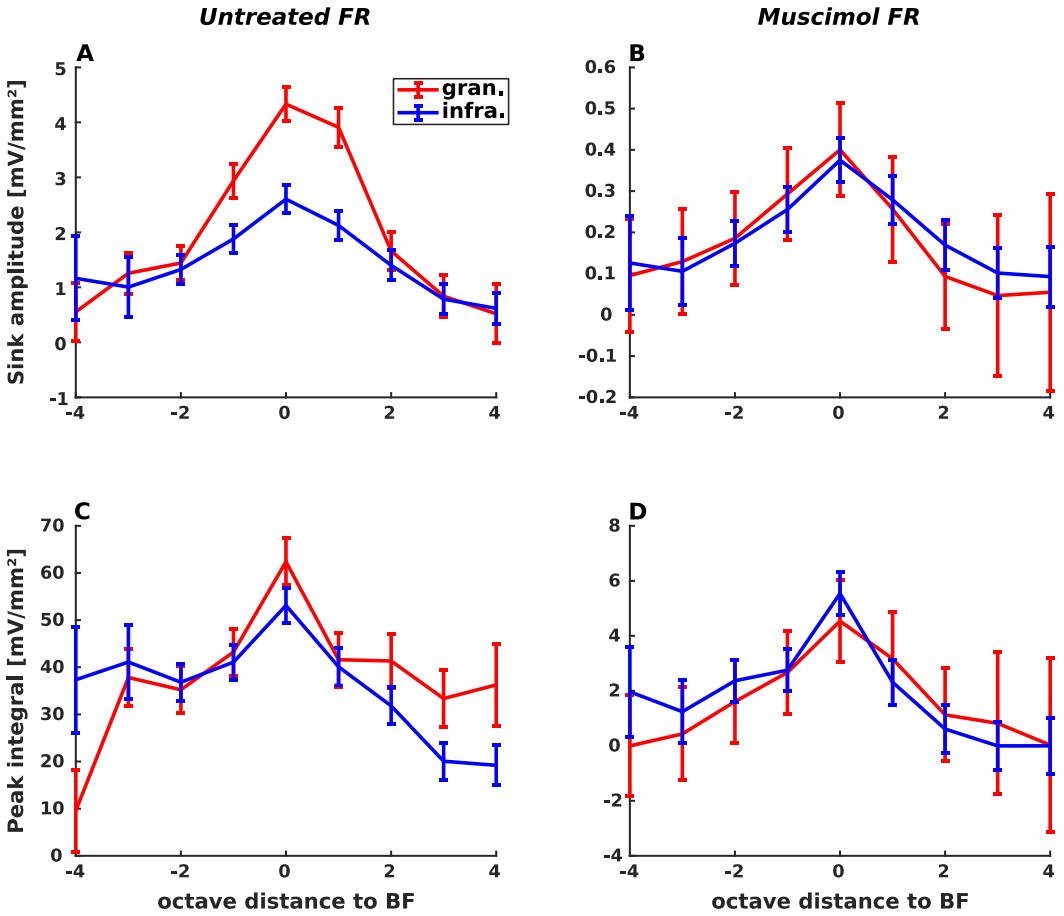

Figure 3. 2 Grand mean of layer-specific FR functions

Sink amplitude and peak integral of initial granular (*red*) and infragranular (*blue*) sink activity are plotted against audio frequency, in octave distance from the BF. Grand mean of the sink amplitude (n = 9) in the *Untreated FR* condition (**A**) and the *Muscimol FR* (**B**) recordings. Note the different scales of the ordinates. Grand mean of the peak integral (n = 9) in the *Untreated FR* (**C**) and the *Muscimol FR* (**D**) recordings.

In order to characterize the audio frequency dependence of the response of granular and infragranular sinks, at the group level, the grand mean of the layer-specific FR function was determined from the sink amplitude and for the peak integral, for both untreated and muscimol recordings. Sink amplitudes reflect the instantaneous maximum inflow of excitatory synaptic mass current in each layer in response to a tone. The peak integral is a measure of the total sink current flowing across the membranes, and its peak latency reflects the termination latency of the sink activity. In this work, the peak integral was calculated for the first 100 ms after tone onset, which corresponds to the tone duration.

Figures 3.2A and 3.2B show, for the two layers and both states, a clear maximum at BF, although in the *Muscimol FR* recording the response strength in the two layers is about one

order of magnitude smaller than in the *Untreated FR* recording. In the untreated state (Figure 3.2A), the curve of the FR function is sharper in the granular layer compared to the rather flat curve of the infragranular layer. This difference between the two layers vanished after the application of muscimol (Figure 3.2B), which may indicate that, in the untreated case, the cortical circuitry selectively amplifies the response to the BF and near-BF stimuli within the granular layer.

The grand mean of the sink integrals (Figures 3.2C and 3.2D) also show a maximum at BF in the granular and infragranular layers and the two conditions. Interestingly, the difference between granular and infragranular layers as displayed in Figure 3.2 A became much weaker in Figure 3.2C, i.e. no such selective granular amplification was found for the peak integral as it was the case for for the sink amplitude. This comparison indicates that the stronger sink activation in the granular layer reflected by the larger sink amplitudes were mainly due to a stronger synchronization of synaptic events in granular layers rather than due to an increase of the overall synaptic currents.

3.2 SOI-dependent responses properties to repeated tone stimulation

Studies on SSA typically focus on the stimulus-specific aspect of adaptation; therefore, the oddball paradigm is commonly used for highlighting the stronger deviant response in comparison to the standard responses that are gradually decaying with repetitive stimulation. RS is a fundamental aspect of SSA, which reveals the attenuation of responses to repetitive stimulation, and its SOI-dependence can be viewed as a temporal filtering characteristic of auditory adaptation.

In order to quantify the SOI dependence of RS kinetics, the regular-SOI paradigm was applied with repetitive tones (BF or non-BF) being presented in blocks of sequences with systematically varying SOIs, both before and after cortical silencing. During a sequence of tone stimulation, the response strength decays gradually, typically within the first 2 s, and then approaches a stabilized level. CSD response traces to single tones were extracted from this steady state of the RS sequence for each SOI by averaging the CSD across trials (n=24), channels covering the respective initial sinks of the granular and the infragranular layers, and single tone epochs with latencies > 2s after sequence onset. During the RS measurements in the untreated state, both BF and non-BF tones were presented, therefore the combinations of state and

stimulus is referred to as untreated BF and untreated non-BF conditions, respectively; under muscimol, only BF was presented, which will be referred to as muscimol BF condition.

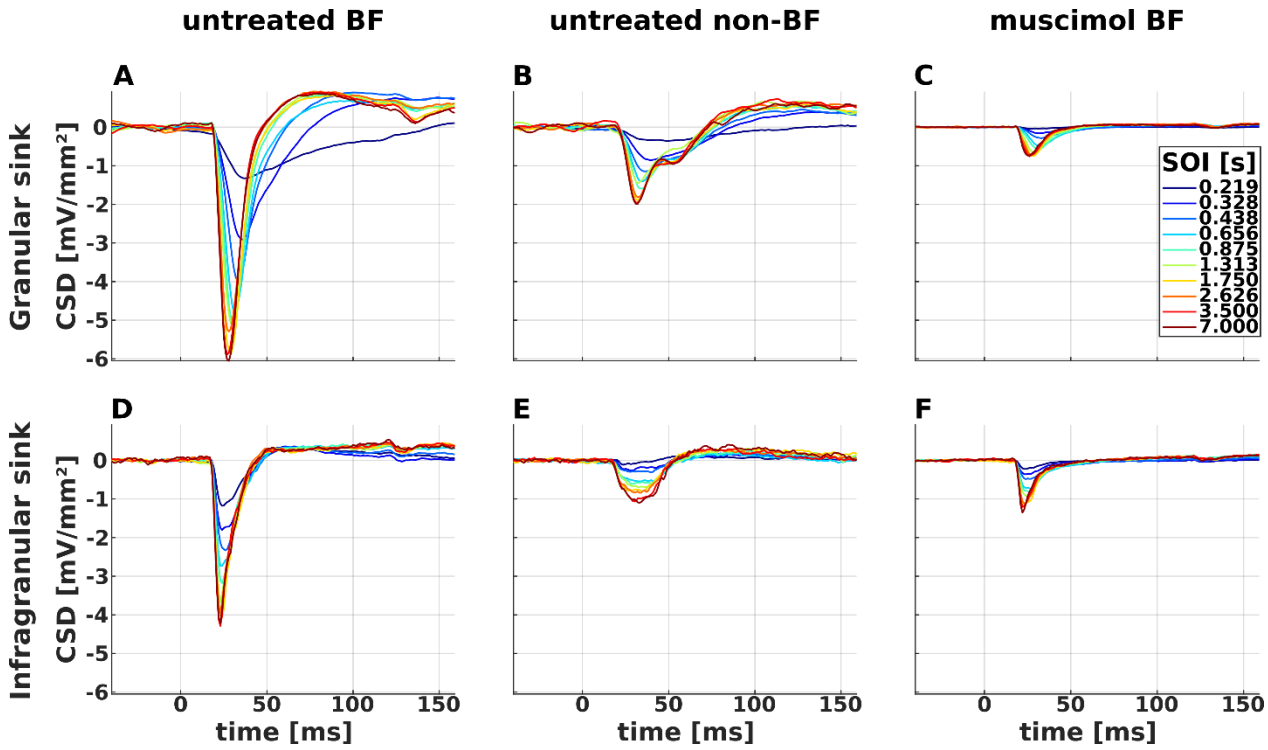

Figure 3. 3 Single-subject example of the SOI dependence of sink response

Tone-evoked sink activity reflected by the layer-specific CSD traces in the steady state, were averaged across stimuli for granular (**A**, **B** and **C**) and infragranular (**D**, **E** and **F**) sinks. SOI dependent traces are displayed for untreated BF (**A**, **D**), untreated non-BF (**B**, **E**), and muscimol BF (**C**, **F**) conditions. SOIs are color-coded in the legend to **C**, which applies to all subpanels.

Figure 3.3 shows for a single subject, the SOI-dependence of the layer-specific response for each condition (untreated BF, untreated non-BF, muscimol BF) for a time window from -40 ms to 160 ms relative to tone onset. Response waveforms were similar to those shown for the FR measurement (Figure 3.1C and 3.1D) with dominant negative peaks in the granular and infragranular layer reflecting initial sinks. In both layers and for all three conditions, the response strength increases with increasing SOI. In the granular layer (Figure 3.3A, 3.3B and 3.3C), it can be seen that the peak latency decreases with increasing SOI as well. The correlation between the sink amplitude and the peak latency will be systematically and statistically analyzed in a later Figure 3.5. For both BF (Figure 3.3A and 3.3D) and non-BF stimuli (Figure 3.3B and 3.3E), the general response strength is larger for the granular layer compared to the infragranular layer. After cortical silencing (Figure 3.3C and 3.3F), the difference in the response strength between the two layers decreased. Moreover, the response duration reflected by the width of the

peak/waveform decreased. Within each layer, the response strength in the *Untreated RS* recordings was larger during BF stimulation (Figure 3.3, left panel) than during non-BF stimulation (Figure 3.3, middle panel), and it further decreased in the *Muscimol RS* recordings (Figure 3.3, right panel).

As the onset and duration of sink activation were highly variable, I calculated the cumulative sum as a means to determine the total sink current (see Methods). Layer-specific cortical CSD-responses are generated by a large mass of synaptic events. The peak amplitude of the cortical sink response thereby depends on the amount of synaptic current flow, which in turn depends on the number of pre-synaptic events, and the gain of the activated synapses. Moreover, as the peak of the sink marks the maximum current flow at one point in time, i.e. the peak latency, it thus also relies on the synchronization of synaptic events. As the reduction of the peak amplitude is a feature of decreasing SOI, it remains unclear, whether or to which degree RS leads to a reduction of synchronization of synaptic events that is reflected by the sink amplitude, or to a reduction of the total synaptic current flow. To disentangle the contribution of these two mechanisms, the overall amount of sink current was quantified by calculating the sink integral (see Methods).

Figure 3.4 shows, for the same animal as in Figure 3.3, the sink integral of the CSD in the granular and infragranular layer, and for all three conditions, was obtained. The peak of the waveform marks the total sink current amount during the sink activation, i.e. peak integral. The latency of the peak reflects the duration from stimulus onset to the end of the sink activation. The peak integral is also dependent on SOI, but the dependence is less strong as for the sink activation (Figure 3.3). In both layers and all the conditions, the peak integral decreases with decreasing SOI, with only a few exceptions. The peak integral is larger for the granular than for the infragranular layer for the *Untreated RS* recordings, both for BF (Figure 3.4A and 3.4D) and non-BF stimulation (Figure 3.4B and 3.4E). However, the waveform shape and the size of the sink integral of granular and infragranular layers became more similar after cortical silencing (Figure 3.4C and 3.4F).

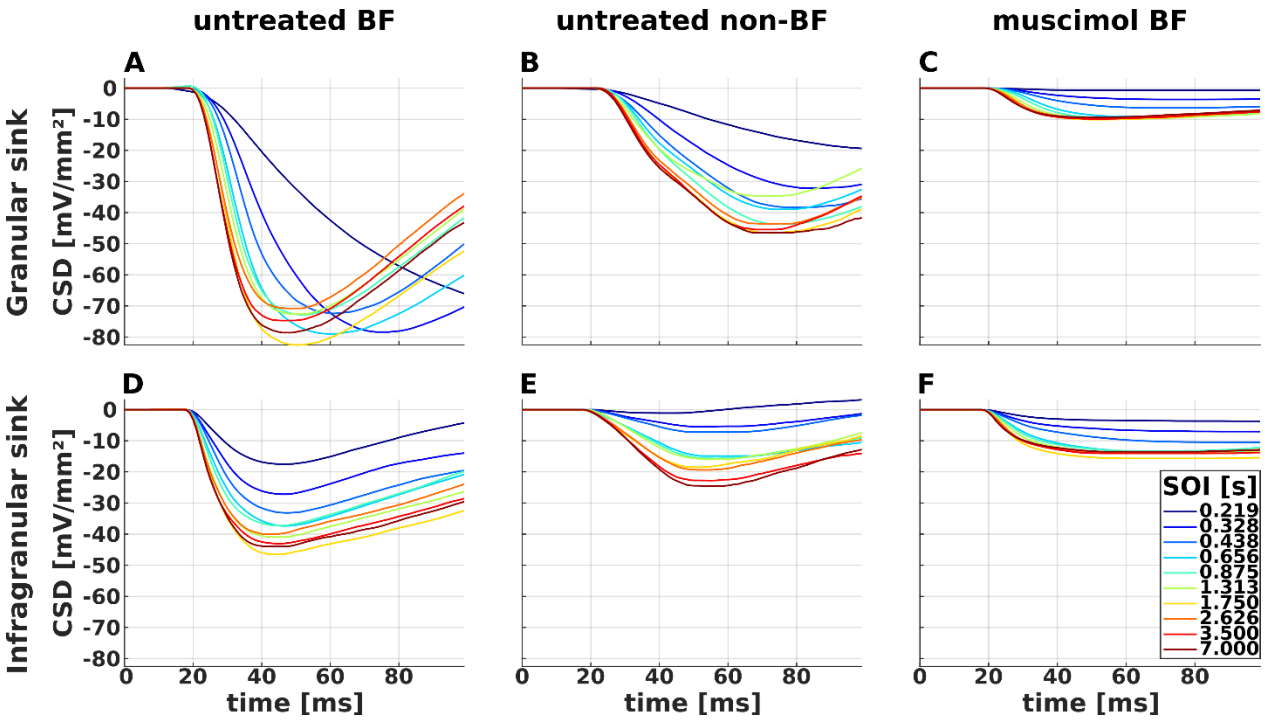

Figure 3. 4 Single subject example of SOI dependence of the sink integral (*same subject as in Figure 3.3*)

The cumulative sum of the inward positive current flow was calculated for the first 100 ms after tone onset, as a measure of sink integral for both of the granular (*upper panels*) and infragranular (*lower panels*) layer, and for untreated BF (**A** and **D**), untreated non-BF (**B** and **E**) and muscimol BF (**C** and **F**). SOIs are color-coded in the legend to **F**, which applies to all subpanels.

In the left and middle panels, the sink integral first decreases until a minimum, and then gradually increases. During the whole timespan of sink activation, negative sink currents are flowing from the extra- into the intracellular space, and the amount of negative currents override the positive currents of the balancing sources, therefore the sink integral continuously decreases. If no later sources occur, the cumulative sum remains at a negative plateau, as it is the case for the muscimol BF condition, see Figures 3.4C and 3.4F. If there are later positive source current, the sink integral starts to increase, and displays a negative peak, which marks the time point when the sink ends. In both cases, i.e. either with a clearly visible peak (Figures 3.4A, B, D, E) or with a plateau (Figures 3.4C, F), the minimum of the cumulative sum is a good estimator for the total sink current, i.e. the sink current summed up to the time point when the sink terminates. For both granular and infragranular layers, the amount of sink integral is larger during BF stimulation (Figure 3.4A and 3.4D) than non-BF stimulation (Figure 3.B and 3.4E). In both granular and infragranular layers, the sink integral reaches its minimum earlier during BF stimulation compared to non-BF stimulation. This suggests that after BF-stimulation, the sink

terminates earlier than after non-BF stimulation. The later part of the sink integral trace was not the focus, and it is therefore not fully presented by the 100 ms time window during which it was calculated.

After cortical silencing, the amount of the sink integral was largely reduced in both layers. In contrast to the untreated conditions with either BF or non-BF stimulation, the sink integral traces showed no peak, but a lower plateau, consistent with the finding, that there were no response components in the CSD traces at latencies > 40 ms. Notably, the difference of the sink integral between granular and infragranular layers as observed in the untreated conditions largely diminished after treatment with muscimol (compare Figure 3.4C with Figure 3.4F).

The single-subject data shown in Figure 3.3 indicate that during sink activation, both the sink amplitude and the peak latency of the layer-specific CSD traces are sensitive to SOI. Specifically, the peak amplitude decreases with decreasing SOI, the peak latency increases, suggesting an inverse correlation between peak amplitude and peak latency. In order to analyze the correlation between the peak amplitude and peak latency of the CSD traces at group level, the grand mean of the peak amplitudes of the CSD traces are plotted as a function of the corresponding grand mean of the peak latencies in Figure 3.5. These grand means were calculated by averaging across the individual medians, which were derived from the bootstrap analysis (Efron, 1979) as described in Section 2.4.5.

Decreasing sink amplitudes with decreasing SOIs are always accompanied by an increase of the peak latency (Figure 3.5), which displayed, to a good approximation, a linear, negative relationship between peak amplitude and peak latency in both granular (dots) and infragranular (triangles) layers in all three panels. Correlation analysis revealed significant negative correlations between sink amplitude and peak latency. Common correlation coefficients averaged via Fischer's z-transform across animals were significantly larger than zero in all conditions with mean values larger than 0.6 (Student t-tests of Fischer z-values across subjects, $p < 0.03$, untreated BF: $r_{gran} = -0.9$, $r_{infra} = -0.8$; untreated non-BF: $r_{gran} = -0.7$, $r_{infra} = -0.7$; muscimol + BF: $r_{gran} = -0.8$, $r_{infra} = -0.6$). Linear regression analysis also revealed a constant latency difference of about 5 ms between granular and infragranular sinks across all SOIs, at untreated BF condition (Figure 3.5A). During untreated non-BF condition, the peak latency difference between the two sinks was also 5 ms for larger SOIs, but then increased with decreasing SOI to about 15 ms at the shortest SOI = 0.219 s (Figure 3.5B). Under muscimol condition (Figure 3.5C),

BF stimulation lead to a constant latency difference of around 6 ms between the granular and the infragranular sinks across SOIs, similar to that observed for the untreated BF condition in Figure 3.5A. These findings indicate the importance of the timing of synaptic events in RS.

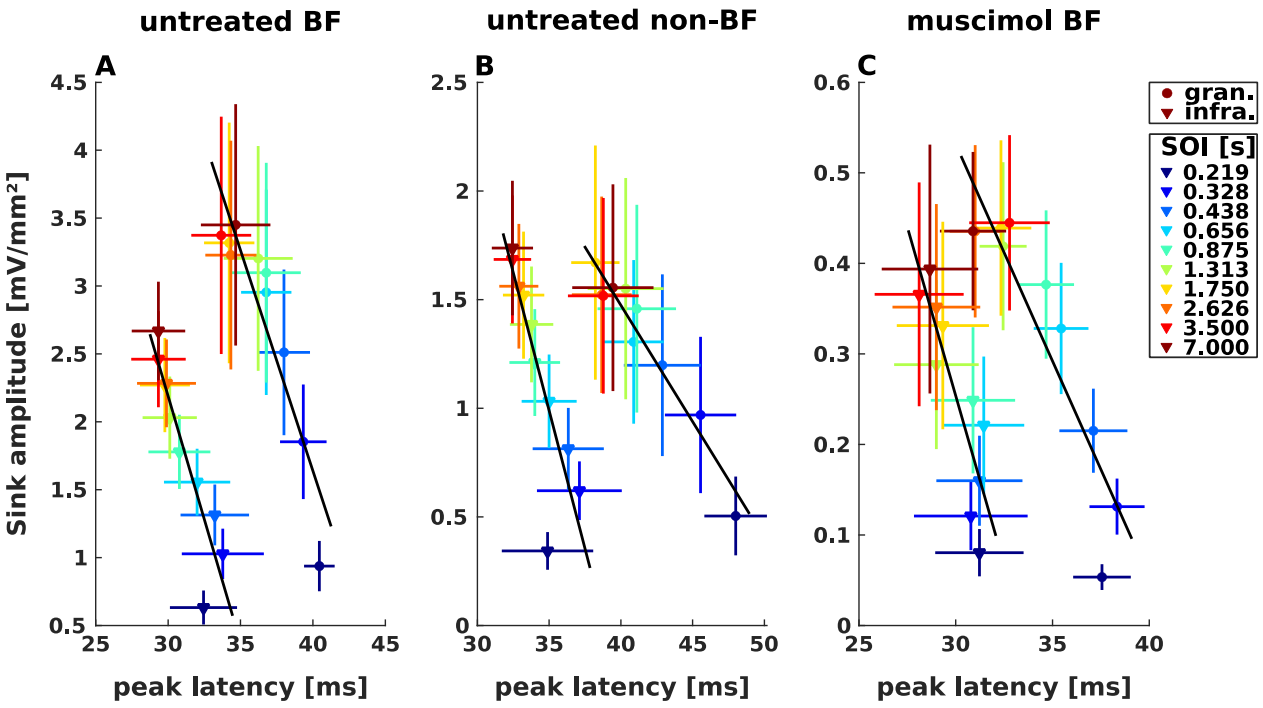

Figure 3. 5 Relationship between peak amplitude and peak latency of sink response (grand mean)

A. For each SOI (*color coded*), the grand mean peak amplitudes and their 95% CIs (*vertical bars*) are plotted against the corresponding peak latencies and their 95% CIs (*horizontal bars*), for granular (*dots*) and infragranular (*triangles*) layers at BF stimulation during *untreated RS* recordings. The black lines present the linear fits to the grand means, performed separately for each layer. **B.** as **A** for the non-BF stimulation during *untreated RS* recordings. **C.** as **A** for the BF stimulation under *muscimol RS* recordings. Note the different scaling in both axes across the three panels.

3.3 Kinetics of RS characterized by estimation of time constant via exponential fitting

Figure 3.3 showed a dependence of RS on the SOI value (Lü et al., 1992; Lu et al., 1992; Zacharias et al., 2012). To quantify the RS kinetics, i.e. the change of sink activity as a function of SOI, for each individual subject, an exponential function (Equation 2, based on Lu et al., 1992; Zacharias et al., 2012) was fitted separately to the granular and infragranular response measures, i.e. the peak amplitude of the sink activity — sink amplitude (see Figure 3.3) as well as the peak amplitude of the sink integral — peak integral (see Figure 3.4). The fitting approache using the exponential function in Equation 3 allows for characterizing the RS kinetics by two free

fitting parameters, the time constant τ and the saturation level *A* (see Methods). Graphically, the time constant τ indexes the steepness of the exponential function of the RS kinetics. Physiologically, τ is a measure of the lifetime of RS. With a short τ, response recovers to its saturation level at a short SOI. Therefore, short τ indicates more short-lived RS, longer τ more long-lived RS. Visually, the steeper the exponential curve, the shorter the time constant τ. Moreover, τ can be interpreted as the temporal scale of RS, and thus as its temporal filtering characteristics: with larger τ values, RS reduces neural responses at longer time scales, during this suppression mechanism larger range of information is filtered out, e.g. timing information. The saturation level *A* is the neural response strength that is asymptotically reached at infinitely long SOIs, i.e. the response strength being not influenced by preceding stimuli.

As shown in the upper panel of Figure 3.6 A-C, for a single subject, the median of the response waveform in red falls in the middle range of the resampled response curves shown in gray. Also, the median sink peak shown as a red point falls in the middle range of the resampled peaks displayed as black points. This indicates that the bootstrap analysis helps to reduce the influence of possible outliers yielding a robust estimation of CSD responses and fitting parameters. The bootstrap method also provides CIs of waveforms and response measures for each single animal. As for the lower panel (Figure 3.6 D-F), for the same subject, resampled (black points) and median (red points) sink peaks obtained from the responses are shown for each SOI. The sink amplitudes increase and saturate at longer SOIs. The exponential model was fitted separately to each set of resampled sink amplitudes as function of SOI. Fitted curves are displayed in gray. The red curves show the exponential function obtained for the median parameter values (median time constant, and median saturation). Median sink amplitudes shown as red dots are all close to the median fitting curve shown in red. This confirms the exponential relationship between the sink amplitudes and SOI. Comparing the exponential fitting curve for the granular layers at BF stimulation during *Untreated RS* and *Muscimol RS* recordings, besides in general larger amplitude before cortical silencing, the exponential fitting curves in the untreated state are steeper which indicates a shorter τ. The values of the time constant τ derived for different layers and subjects will be more systematically compared in the following.

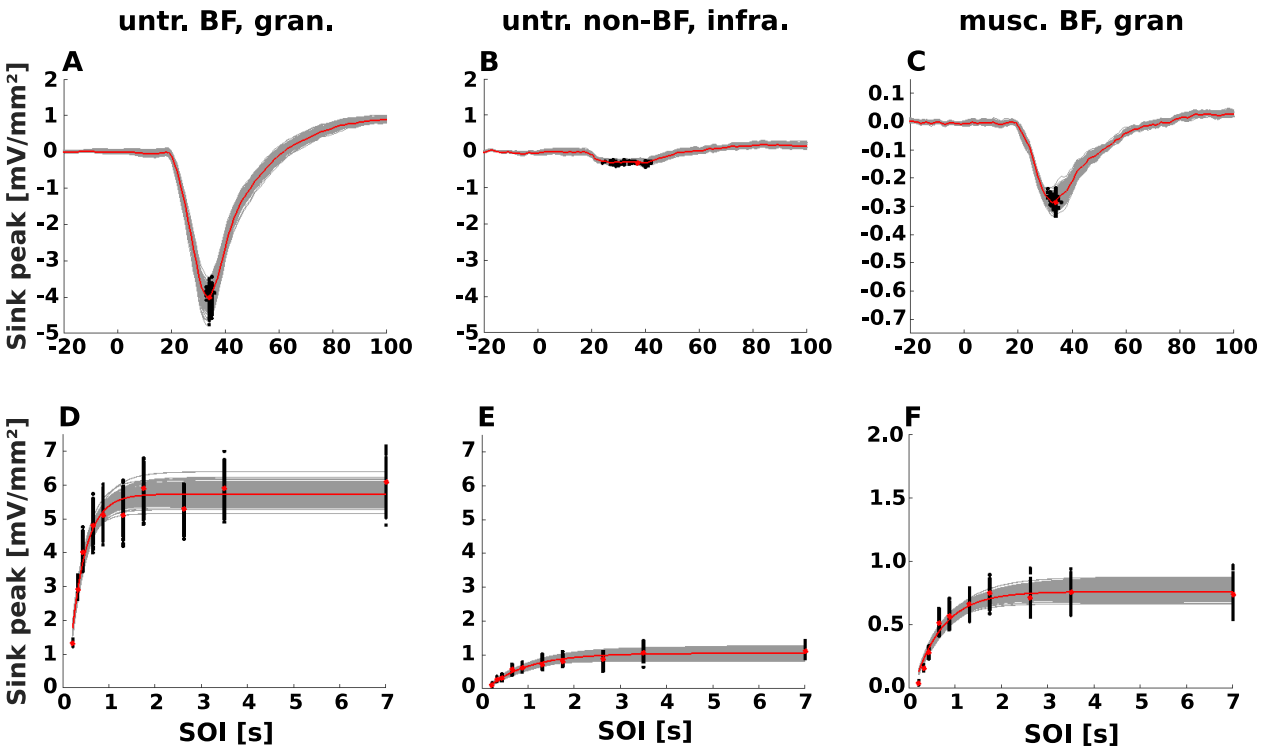

Figure 3. 6 Exponential fitting of RS kinetics of sink activity (*same subject as in Figure 3.3*)

A - **C** show the 1000 bootstrap random samples of stabilized layer-specific CSD traces (*gray curves*), from -20 to 100 ms re tone onset at a SOI of 0.438 s, with individually detected peaks plotted in *black dots*, for **A** the granular layer in the untreated BF condition, **B** the infragranular layer in untreated non-BF condition, and **C** the granular layer under muscimol BF condition. The median waveform of the 1000 waveforms and its peak are plotted in red. **D** - **F** presents the peak amplitudes (*black dots*) of all bootstrap samples shown in **A** to **C** as a function of SOI, for **D** the granular layer during untreated BF condition, **E** the infragranular layer under untreated non-BF condition, and **F** the granular layer during muscimol BF condition. For each SOI, the 1000 bootstrap samples are displayed in *black dots*, and the *gray curves* are the corresponding exponential fitting curves (Equation 3). *Red dots* indicate the median peak amplitudes across the 1000 random samples, and the *red curves* display the corresponding exponential fitting curves.

In order to investigate the potential cortical influences on the RS kinetics of sink activity on a layer-specific manner, the life time indexed by τ of RS is systematically compared for one subject, between layers and among conditions. In Figure 3.7, the median τ values of granular layer are plotted against that of infragranular layer in dots, color coded for each subject.

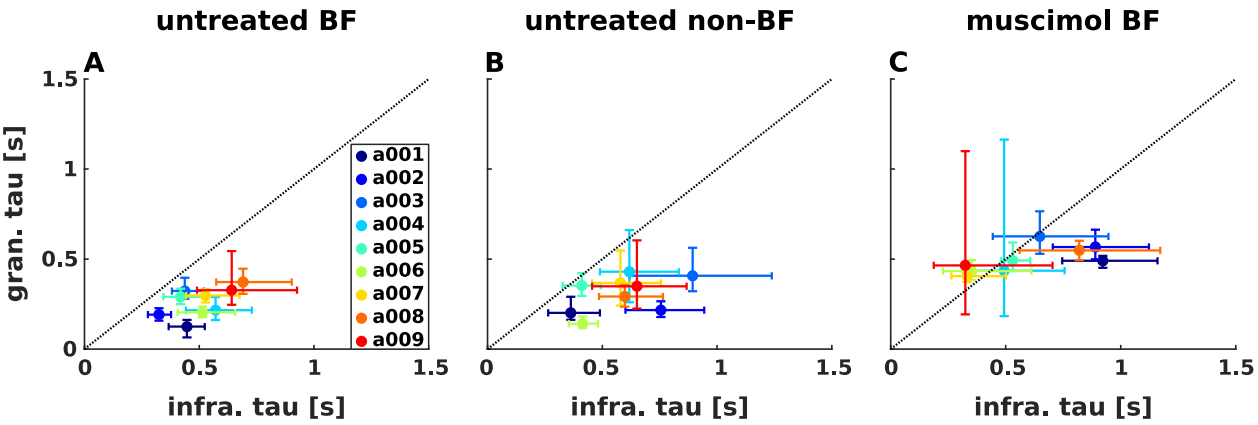

Figure 3. 7 Comparing lifetime of RS between granular and infragranular layers

Time constant τ of granular layer is plotted against that of infragranular layer, color coded for each subject, for untreated BF (**A**), untreated non-BF (**B**) and muscimol BF (**C**) conditions. Time constants are displayed as the medians (see Methods). 95% CIs of the time constants are indicated by *vertical* (granular) and *horizontal* (infragranular) *bars*. The *black-dashed bisecting* line marks equal τ-values between the two sinks.

In the untreated BF condition (Figure 3.7A), the τ values in the granular layer were shorter than in the infragranular layer, in all nine animals, i.e. all the medians and CIs fell below the bisecting line. This indicates a more short-lived RS of the granular compared to the infragranular sink. In the untreated non-BF condition (Figure 3.7B), seven out of nine animals displayed shorter τ values in granular layer with CIs of just two animals slightly crossing the bisecting line. However, in the muscimol BF condition (Figure 3.7C), most of the data points shifted closer to the bisecting line, compared to the untreated BF condition. The CIs of six out of nine subjects clearly expand and cross the bisecting line. Notably, CIs are much larger in the Muscimol BF condition, most likely due to the small peak amplitudes and the corresponding smaller signal-to-noise ratio of the response.

Comparing the layer-specitic τ values across conditions, in the granular layer τ was clearly prolonged by cortical silencing with muscimol (Figure 3.7A and 3.7C). On the other hand, within the infragranular layer, τ values showed no consistent changes across conditions, except for an increase of the CIs by non-BF stimulation (Figure 3.7B) and application of muscimol (Figure 3.7C). As discussed in the introduction, the sink activity after cortical silencing with muscimol mainly reflects afferent thalamocortical inputs while intracortical contribution are inhibited. Therefore, comparing the untreated BF and muscimol BF (Figure 3.7C) conditions, the shorter τ value in the granular layer with cortical processing (Figure 3.7A) suggests that the intracortical processing reduces the lifetime of the RS kinetics via enhancing already adapted thalamocortical

inputs. No such effects of changing the RS kinetics by cortical silencing was found in the infragranular layer.

In order to further investigate, whether the observations of the layer-specific time constants, derived from sink activity, as well as the intracortical shortening the time constant τ in the granular layer (Figure 3.7), also statistically hold at the group level, a group statistical analysis was carried out. The results are shown in Figure 3.8A. In the untreated state, the granular layer displayed shorter τ values compared to the infragranular layer, for both BF and non-BF stimulation. At the BF stimulation, the time constants (grand mean +/- SEM) were τ_{gran} = (0.261 ± 0.025) s and τ_{infra} = (0.508 ± 0.038) s, whereas for the non-BF stimulation, τ_{gran} = (0.306 ± 0.034) s and τ_{infra} = (0.585 ± 0.058) s). In the muscimol BF condition, the time constant of the granular layer with τ_{gran} = (0.503 ± 0.023) s was by a factor of about two larger than at untreated BF condition, close to the value for the infragranular layer with τ_{infra} = (0.586 ± 0.079) s, i.e. which was almost unaffected by the application of muscimol. Apparently, cortical silencing changed the life time of RS in the granular sink, but little in the infragranular sink. Friedman's test showed significant changes ($\chi^{2v}_{df=5}$ = 27.3, p = $6 \cdot 10^{-5}$) across layers (granular and infragranular) and conditions (BF, nonBF, and muscimol + BF) for the repeated measures within subjects. Bonferroni-corrected post-hoc testing revealed significantly shorter time constants in the granular layer under BF stimulation compared to the other two conditions ($p < 0.03$).

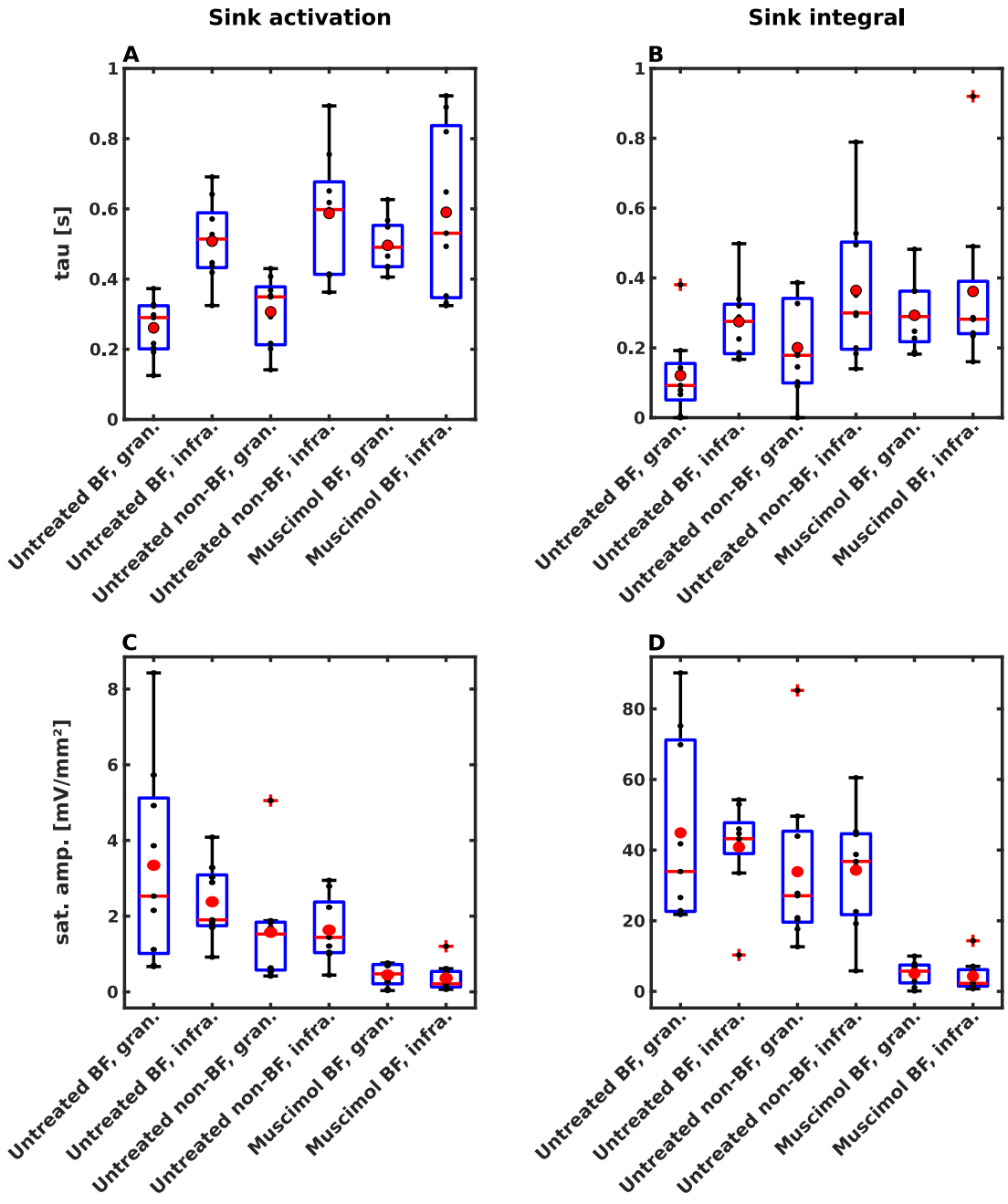

Figure 3. 8 Distribution of time constants and saturation amplitudes across subjects

The upper panels **A** and **B** display the distribution of estimated time constant $\boldsymbol{\tau}$ of the RS kinetics across animals for the peak amplitude of sink activity (maximum sink current, **A**), and the peak amplitude of sink integral (total sink current, **B**) of both the granular and the infragranular sinks, for the untreated BF, untreated non-BF, and muscimol BF conditions. The median values for each animal are plotted as black dots with the black dash line showing the range of median values of the whole group (n=9). 95% CIs of the 9 subjects are plotted as blue box, and outliers are marked by *red-cross*. Within each blue box, the red dot displays the grand mean across subjects and the red line the grand mean of medians across animals. The lower panels show the distribution of the estimated saturation level $\boldsymbol{A}$ across animals for the sink activation (**C**), and the sink integral (**D**) of the granular and the infragranular sinks, for all three conditions. For each animal, median parameters $\boldsymbol{\tau}$ and $\boldsymbol{A}$ were selected across the 1000 resampled curve fits, in order to obtain a robust estimation (see section 3.3.1).

As a second free fitting parameter, the saturation level *A* of sink amplitudes (Figure 3.8C) was also investigated and showed overlapping values between granular and infragranular layers

in all three conditions. However, within each layer, *A* decreased from untreated BF to untreated non-BF condition and was, as expected, smallest for the muscimol BF condition. Friedman's test showed highly significant changes ($\chi^{2v}_{df=5}$= 31.4, p = 8*10^{-6}) for within-subject factors layer (granular/infragranular), stimuli (BF/non-BF) and states (untreated/muscimol). For both the granular and infragranular sinks, Bonferroni-corrected post-hoc t-tests revealed significantly smaller saturation level *A* under muscimol BF condition comparing to BF (p < 0.004), whereas intermediate saturation level *A* at untreated non-BF condition. These results indicate that the life time of RS revealed by the time constant τ does not depend on the saturation level *A*.

3.4 Response properties related to RS

Figure 3.3 and Figure 3.4 showed that although both of the sink activation and sink integral were SOI dependent, the peak amplitude of the sink activation still clearly show a stronger SOI dependence. The sink activation is generated as mass event consisting of multiple synchronous synaptic events. The sink amplitude thereby depends not only on the total number of synaptic events, but also their coincidence. On this basis, the RS of the peak amplitude could arise a decrease of the number synaptic events, and/or a desynchronization of synaptic events. To examine whether the cortical shaping of the lifetime of the RS derived from the sink amplitudes is solely dependent on the RS of the sink integral, the same fitting procedure as done for the sink amplitudes (Figure 3.6) was also done for the peak integral individually and then analyzed statistically at a group level (see Figure 3.8B and 3.8D).

Similar as for the sink amplitude, Friedman's test still showed significant changes of peak integral time constants across layers (granular and infragranular) and conditions (untreated BF, untreated nonBF, and muscimol BF) for the repeated measures within subjects. In line with the observations in sink activity, Figure 3.8B displays the shortest time constant for the granular sink in response to BF stimulation in the untreated state τ_{gran} = (0.118 ± 0.039) s. The time constant of the infragranular sink was longer τ_{infra} = (0.253 ± 0.032) s). Also, longer time constants were observed with non-BF stimulation at untreated state (τ_{gran} = (0.200 ± 0.046) s and τ_{infra} = (0.346 ± 0.070) s). After cortical silencing by muscimol, the time constant of the granular sink was prolonged becoming similar to the time constant of the infragranular sink, which did not change by muscimol treatment (muscimol BF condition: τ_{gran} = (0.291 ± 0.031) s and τ_{infra} = (0.357 ± 0.079) s). Notably, the time constants derived from the peak integral in both layers and all

conditions were shorter than the corresponding values derived from sink amplitude. This indicates that RS is not only due to the suppression of the total amount of synaptic events, e.g. by synaptic gain regulation, but also to a great part to the synchronization of synaptic events in response to repetitive stimulation.

As a second free fitting parameter, the saturation level *A* of peak integral (Figure 3.8D) showed overlapping values between layers in all three conditions, which is in line with that of the sink amplitude (Figure 3.8B). A strong and significant decrease of the saturation level is seen in both layers with muscimol treatment.

In principle, the observed layer-specific lifetime of RS might not be specifically due to layer differences and to differences in cortical processing across layers. They could simply arise from differences in the saturation level *A* of responses across layers and conditions. Also, varying time constants could be generated from fitting bias based on different signal to noise ratios at different response levels. Particularly at shorter SOIs and during cortical silencing, responses can become very small, close to the noise level. To examine whether the time constant τ is indeed dependent on the saturation level *A*, a correlation analysis was carried out for the sink peak in individual animals across the 1000 resampled estimates of saturated amplitudes obtained by bootstrapping (see point clouds, in Figure 3.9A colored differently for each animal).

Figure 3.9A presents that, irrespective of layer and condition, higher saturation amplitudes were, in all animals, significantly positively correlated with longer time constants (Figure 3.9A), with a common correlation coefficient > 0.7 that was significantly larger than zero in all conditions ($p < 0.00002$). In contrast to this correlation, increased response levels across layers and experimental conditions were rather associated with shorter time constant (Figure 3.9B). For instance, in the untreated BF condition, the granular sink (red square) with its larger saturation amplitude, has a shorter time constant, compared to the infragranular sink (blue square). Thus, experimental effects were opposite to the trend shown in Figure 3.9A. Thus, the observed significant differences in time constants across layers and conditions apparently are genuine layer effects, and cannot be simply explained by differences in the saturation amplitudes between layers.

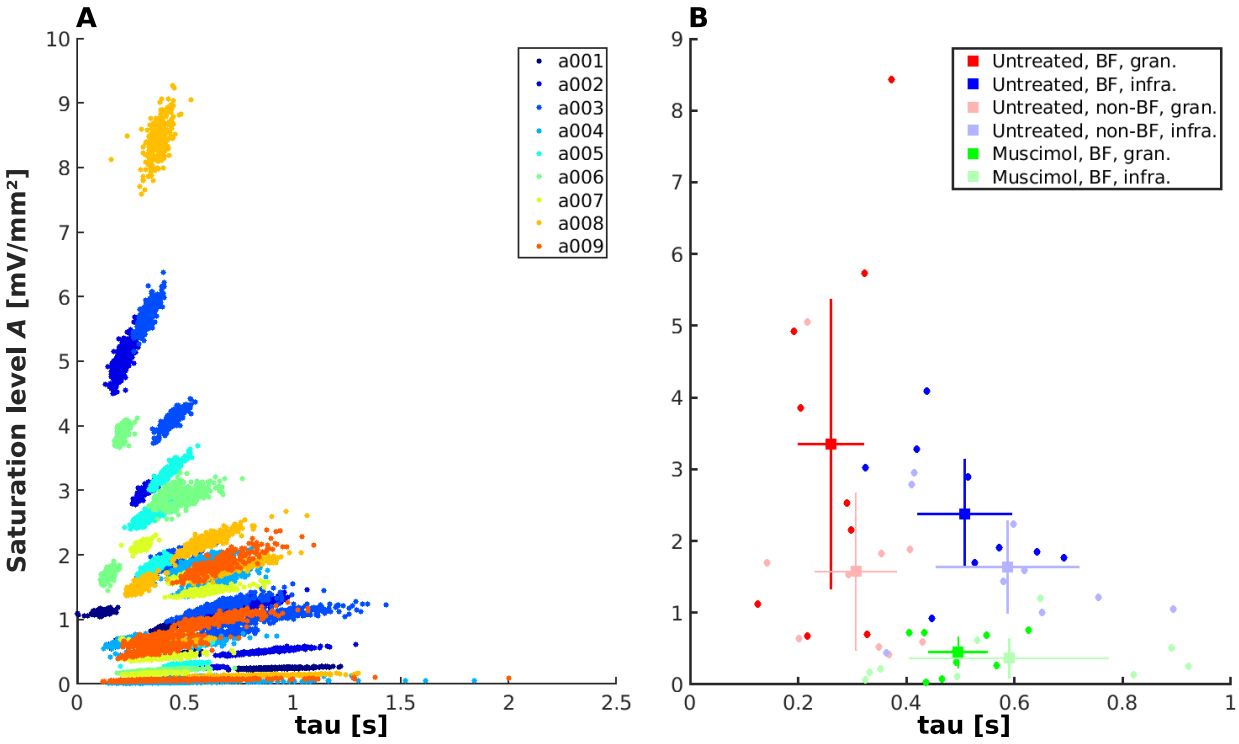

Figure 3. 9 Relationship between saturation amplitude *A* and time constant τ

A. For each subject (*color coded*), the two layers (granular and infragranular) and the three conditions (untreated BF, untreated non-BF and muscimol BF), the saturation level *A* was plotted against the time constant τ for all the 1000 bootstrapping samples, which resulted in six *data clouds* per subject representing the six combinations of layer and condition. **B.** Correlation between the median saturation amplitude *A* and median time constant τ. The median saturation amplitude was plotted against time constant for each subject in *dots*, combinations of layer and experimental condition are color coded. Grand mean across individual medians were plotted in *squares*. 95% CIs of saturation amplitudes and time constants are shown by *horizontal and vertical bars*, respectively.

To quantify the strength of RS as function of SOI, an RS index was calculated according to Equation 3, where a_{SOI} is the response strength measured by either sink amplitude or peak integral at the steady state of RS, and A is the estimated saturation amplitude via exponential fitting. In Fig 3.10, SOI-dependent RSI_{SOI} values are plotted for each layer and condition.

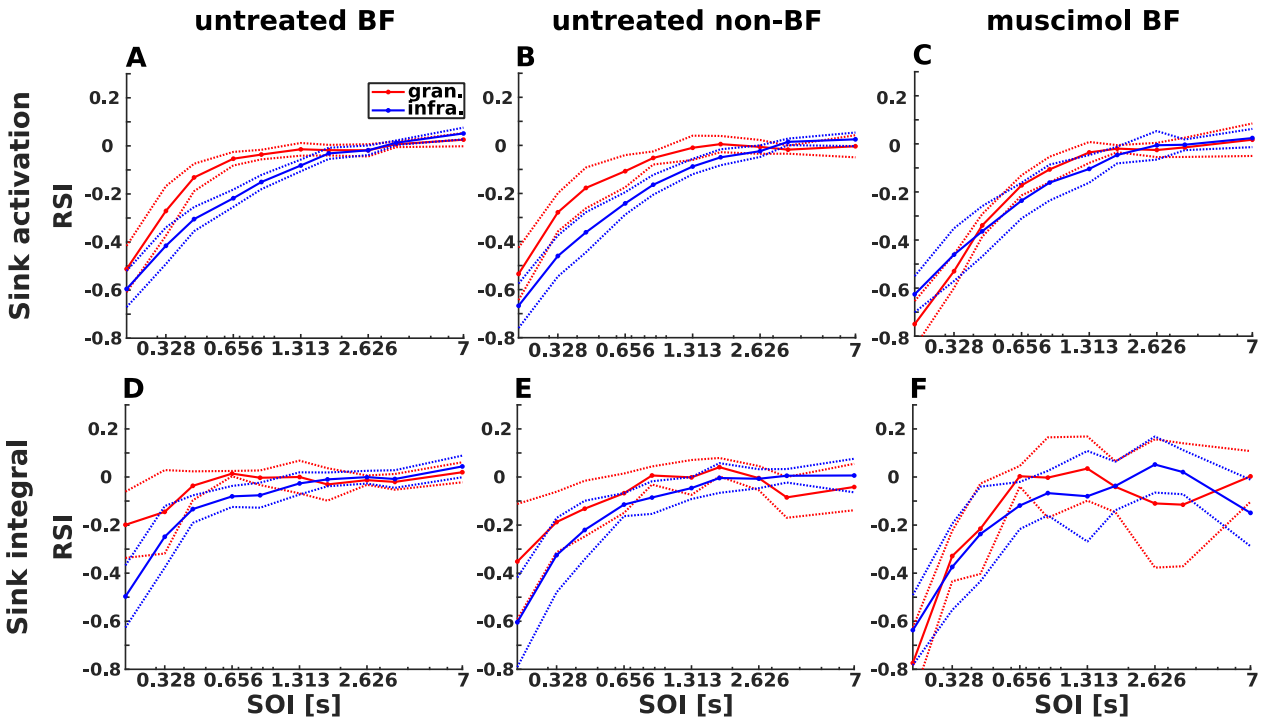

Figure 3. 10 RSI_{SOI} as a function of SOI

Upper panels: RSI_{SOI} values of the sink amplitudes as a function of SOI plotted on a logarithmic axis for granular (*red*) and infragranular (*blue*) layers in the untreated BF (**A**), untreated non-BF (**B**), and muscimol BF (**C**) conditions; ***Lower panels***: RSI_{SOI} values for the peak integral as a function of SOI for granular (*red*) and infragranular (*blue*) layers inthe untreated BF (**D**), untreated non-BF (**E**), and the muscimol BF (**F**) conditions. Negative RSI_{SOI} indicates suppression and positive RSI_{SOI} facilitation of the response relative to the saturation amplitude. When there is no change, then RSI_{SOI} = 0 for that particular SOI. Grand mean RSI_{SOI} (*solid curves*) across animals (n = 9) and their 95% CIs (*dotted curves*) are shown as a function of SOI for both sinks.

For the sink amplitude (Figure 3.10, upper panels), clear suppression with negative RSI_{SOI} was found for all conditions at SOIs < 1 s. In the untreated BF condition (Figure 3.10A), the two layers revealed negative RSI_{SOI} with clearly separated CIs at SOIs between 0.438 s and 1.313 s. This separation between the CIs of each layer is also visible, though less pronounced, during non-BF stimulation (Figure 3.10B). After cortical silencing, the two sinks exhibited similar RSI_{SOI} values with similar SOI dependence (Figure 3.10C).

For the peak integral (Figure 3.10D-F), RSI_{SOI} became negative for SOI < 1 s, in both sinks and all three conditions. During untreated BF condition (Figure 3.10D), in contrast with the sink amplitude, the only significant layer difference was found below a SOI of 0.656 s by a more negative infragranular RSI_{SOI}. However, in the untreated condition (Figure 3.10D and 3.10E, well separated CIs), at SOI value below 1.313s, RSI_{SOI} values in the granular layer were less negative than for the sink amplitude. After cortical silencing, RSI_{SOI} values of the sink integral at SOI <

0.656 s had similar negative values for the sinks in both layers (Figure 3.10F), thus being similar to the RSI_{SOI} of the sink amplitude (Figure 3.10C). However, for the peak integral, RSI_{SOI} values of 0 that indicate full recovery from the preceding stimulation, started at shorter SOIs than for the sink amplitude. This is consistent with the shorter time constants for the sink integral than for the sink amplitude. Thus, sink amplitude showed much stronger RS at even longer SOIs, i.e. a longer RS time constant, than sink integrals. These observations suggest that particularly in granular layers, the evoked overall synaptic current was less reduced by RS than maximum current. This again suggests, that synaptic synchronization strongly contributes to RS.

3.5 Correlation analysis of CSD responses related to different SRS kinetics

The time constant τ derived from the sink amplitudes displayed layer-specific RS kinetics (Figure 3.8A). With intracortical processing being intact, granular RS was more short-lived (shorter τ) than infragranular RS (longer τ), see Figures 3.7 and 3.8. However, the question remains, how during intracortical processing the fast and slow RS kinetics observed in granular and infragranular layers at early latencies < 50 ms affect the synaptic activity at longer latencies across all layers. Therefore, a correlation analysis was carried out to determine for each spatiotemporal point in the CSD profile (time window:-50- 100 ms covering the peak latency of the early sink), whether its CSD values as a function of SOI were stronger correlated with the shorter ($\tau_{gran} \cong 0.2$, BF) or with the longer (τ_{infra}, $\cong 0.5$, BF) life time of RS of the untreated BF condition. The correlation was quantified by calculating the Fisher-z values of the correlation coefficients and their t-value differences.

Figure 3.11A-C shows the t-values for all the spatiotemporal points of the CSD profile, for each condition. Positive t-values indicate stronger correlation with short RS lifetime (color coded in red) and negative t-values stronger correlation with the long RS lifetime (color coded in blue). Differences between correlation with short- and long-lived RS kinetics were statistically evaluated on the basis of t-values using a permutation test (Figure 3.8D-F). The original t-values were then compared to the distribution of upper and lower t-values. For this, the correlation values of short- and long-lived RS kinetics were randomly permuted 1000 times for each subject. For each of the 1000 permutations, t-values of the differences of Fischer-z-transformed correlation coefficients across subjects were calculated, as described above. To avoid multiple testing, one single distribution of upper and lower t-values across all spatiotemporal points was

constructed by selecting only the 2.5% and the 97.5% percentile of the t-values of a permutation (Groppe et al., 2011). Then the original t-values to the distribution of upper and lower t-values were compared. For each spatiotemporal point, significantly higher or lower correlation with the fast or the slow RS kinetics was determined by t-values falling below or exceeding the 2.5% and the 97.5% percentile of the random distribution, respectively.

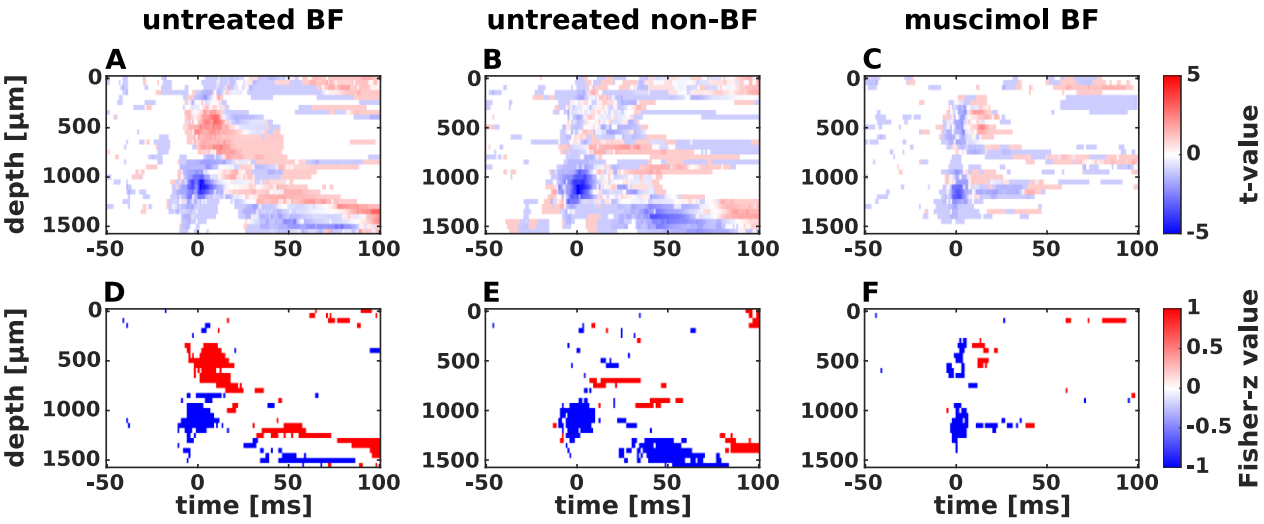

Figure 3. 11 Correlation analysis of fast (shorter τ_{gran}) and slow (longer τ_{infra}) RS kinetics

Upper panel, t-values of the differences of Fischer-z transformed correlation coefficients between the fast granular and the slow infragranular RS kinetics. *Red* codes a stronger correlation with the fast kinetics. *Blue* codes a stronger correlation with the slow kinetics for the untreated BF (**A**), non-BF (**B**), and muscimol BF (**C**) conditions. Non-significant correlations ($p < 0.05$) were set to 0. Note, that time is displayed relative to the peak latency of the sink response. *Lower panel*, the results of a statistical permutation test of the t-values in **A-C** for each spatiotemporal point corrected for multiple testing. *Red patches* indicate significantly higher correlation with the fast kinetics (positive Fisher-z values), and *blue patches* significantly higher correlation with the slow kinetics (negative Fisher-z values). Significant effects are shown for untreated BF (**D**), non-BF (**E**), and muscimol BF (**F**) conditions. To account for variation of response latency across SOIs, the CSD responses were aligned by the peak latency of the infragranular sink.

In the untreated BF condition (Figures 3.11A and 3.11D), CSD showed higher correlation with fast RS kinetics in granular and with slow RS in infragranular layers, consistent with the previous analysis of the initial granular and infragranular sink. However, at longer latencies, fast RS kinetics spread from granular towards infragranular layers. In the untreated BF condition, a significantly higher correlation with the fast kinetics (red) initially in granular layer was found, and from 40 to 100 ms also in infragranular layers. In the non-BF condition (Figures 3.11B and 3.11E), and after application of muscimol with BF stimulation (Figures 3.11C and Fig. 3.11F), CSD responses predominantly showed stronger correlation with slow RS kinetics, even during initial activation in granular layers.

4. Discussion

"Our intuition about how our senses work is that the face of our parents, friends, and loved ones really are as they appear. We believe that our senses convey the true picture of the reality around us in an automatic and uninteresting fashion. Our intuitive faith in our senses hides the fundamental question, do our senses convey reality? I will try to convince you that the way we perceive the world is much more than what is implied in by sayings such as "seeing is believing". Not only is much more going on in our ability to perceive the world than simply making a copy of the outside world in our head, but it is far more interesting."

— John H. Krantz[2]

In summary, the major finding of my study shows that initial granular and infragranular sinks display different repetition suppression (RS) kinetics. The lifetime of the RS in the infragranular sink was nearly twice as long as that of the granular sink. After suppressing the intracortically relayed contributions to the sink inputs by Muscimol, while largely leaving intact the thalamocortical inputs, the lifetime of RS in both layers became comparable with a prolonged time constant in the granular layer and an unchanged time constant in the infragranular layer. This demonstrates an intracortical contribution to RS in the granular layer and raises the suggestion of an intracortical mechanism that re-amplifies the suppressed thalamocortical inputs, therefore effectively reducing the local lifetime of the RS kinetics. Furthermore, for the first time, it was shown that RS was stronger for the sink activation than for the sink integral, indicating an important role of synchronization of synaptic events in RS.

4.1 Methodological considerations

Regular-SOI paradigm and the exponential fitting procedure

SSA has been predominantly examined using oddball paradigms with a focus on characterizing its stimulus specificity as well as the corresponding features like the dependence

[2] *John H. Krantz. Experiencing Sensation and Perception. Upper saddle river, New Jersey: Prentice Hall, 2012.*

of the magnitude of SSA on stimulus probabilities (Ulanovsky et al., 2004; von der Behrens et al., 2009). Essentially, SSA describes relative changes in the response to the standard and the deviant. However, oddball paradigms normally do not distinguish between a response reduction, e.g., to the repetitive standard, and a possible response enhancement towards the rare deviant.

The current study more parsimoniously focuses on the response reduction towards a repetitive stimulus, i.e. RS, which is a fundamental aspect of SSA and MMN and might be a basic mechanism underlying perceptual functions like deviance detection or predictive coding (Nelken, 2014; Ulanovsky et al., 2003, 2004; Winkler et al., 2009). With repeated stimulation, cortical response strength decays gradually until reaching a steady level. Research has shown that this steady level is dependent on an SOI value (Zacharias et al., 2012). Via fixing the SOI within and varying it across trials, the applied regular-SOI paradigm ensures a systematic observation of the SOI dependence on RS level. Combining the exponential fitting approach, the estimated time constant reflects the lifetime of RS, which provides a quantitative measure of RS that could be compared across cortical layers and states.

Initial sinks as observation objects

The early granular and infragranular sinks were of interest as they are located at the layers receiving major thalamocortical inputs, and they are the dominant components of the cortical response and thereby well identifiable. The evoked activation of both sinks involves in two sources of contribution starting with the thalamocortical inputs and later also recruiting the intracortical inputs (Happel et al., 2010). During the untreated state, the intact early granular and infragranular sink activation were seen, as well as the sink and source activities at longer latency. After removal of the corticocortical contribution by muscimol, residuals of early granular and infragranular sinks remain in place with a weaker strength and shorter duration of sink activation, revealing thalamocortical synaptic activation (Happel et al., 2010). The invisible sink and source activation at longer latency that were seen in the untreated state are therefore revealing the intracortical contributions. These evidences confirm that the local synaptic activation can represent different sources of inputs including both thalamocortical and corticocortical contributions.

CSD sinks mainly reflect excitatory synaptic mass currents, whereas sources mainly reflect source currents balancing the sink activities (Happel et al., 2010). At longer latencies, there is

strong superposition of different sinks and sources. The resulting spurious sinks cannot be attributed to a certain population of synapses located in a specific layer. Thus compared to LFP analysis (von der Behrens et al., 2009) or CSD analysis with averaging across longer latency (Szymanski et al., 2009), the current sink-specific response measures are much less confounded by volume conduction or by sources due to return synaptic currents generated in other layers. Assessing this long-latency activity in a layer-specific manner, and in association with local synaptic populations, requires source separation—which is far from trivial. With a simple approach, the correlation analysis specifically assesses positive correlations of CSD activity in other layers and at longer latencies with the early sink activity in dependence on the SOI. Thus, SOI-dependent activity changes were isolated while regressing out negative correlation with superimposed source activity.

Cortical silencing by muscimol

Topical administration of $GABA_A$-agonist muscimol lead to an overall decrease of granular and infragranular responses via inhibiting the intracortical neuronal activity and thus leaving only the brief sink activation resulting from thalamocortical projections (Happel et al., 2010). It has also been suggested that muscimol activates the pre-synaptic $GABA_B$-receptors as well and therefore might weaken the thalamocortical inputs (Yamauchi et al., 2000). However, via a combined application of a cocktail of $GABA_A$-agonist muscimol and $GABA_B$-agonist (SCH50911), Liu et al. (2007) suggested that the residual thalamocortical can be re-enhanced towards levels found in the untreated cortex. However, in a preparation and with measurements similar to my study, Happel et al. (2010) showed that blocking $GABA_B$-receptors did not re-enhance the residual sink activity compared to the mere application of muscimol. Rather, Happel et al. (2010) suggested that muscimol left thalamocortical input largely intact (Deane et al., 2020; Happel et al., 2010; Happel et al., 2014), and that reduction of sink amplitudes after application of muscimol were largely due to a reduction of intracortical amplification.

Advantages of the bootstrapping approach

Theoretically, an average obtained from a larger data set is beneficial for reducing the influence by the signal-to-noise ratio as well as by the outlier trials with response variability. However, the real recording is usually confronted also by extra constraints. As mentioned in the Methods section, a total number of 24 trials of tone sequence were presented with a certain

SOI, stimuli (BF or non-BF), and condition. Such a trial number was a decent compromise between sufficient data and the limitation of total recording time that could be tolerated by the subject with a stabilized physical state, as well as by the experimenter performing at decent levels of concentration. To achieve higher reliability with the existing data, a simple and elegant bootstrapping approach was employed during statistical analysis, at both, the single subject and the population level. The great advantage of bootstrapping is that estimates of standard errors and confidence intervals can be derived in single subjects. Bootstrapping further allows us to control the stability of the data, reduce the influence of outliers, and therefore provide robust estimates—even with a limited amount of data (Davison & Hinkley, 1997)—which is in accordance with the 3Rs principles (Replacement, Reduction, Refinement) in designing and conducting animal experiments (Festing & Altman, 2002; Franco & Olsson, 2014). Moreover, as it is impossible to know the true confidence interval, bootstrapping has been suggested to be asymptotically more accurate than the standard intervals that are obtained by using sample variance and assumptions of normality (DiCiccio & Efron, 1996). It has been shown that from sample sizes greater than 100, negligible improvements in the standard error estimation could be expected (Goodhue et al., 2012). Thus, the chosen sample size of 1000 that is used in the current study was more than sufficient to produce reliable estimates of standard errors and confidence intervals.

Exponential fitting approach

Further, the number of fitting parameters were constrained to time constant τ and saturated amplitude A in order to avoid overfitting, with fixing t_0 at 0.1 s, as explained in Methods. The initial values set for starting the fitting were determined by experience and trials to ensure that the fitting error reached a global minimum instead of just the local minimum. Notably, the main fitting outcome depended neither on the choice of the number of fitting parameters nor on the initial values due to the use of bootstrapping. Reliable fitting was especially crucial for estimating time constant τ after cortical silencing, when the amplitudes of response measure dropped dramatically to bring them close to the noise level. With the current approach, it was demonstrated that the population effects largely held on the single-subject level too.

4.2 Separation of layer-specific subcortical and intracortical contributions to cortical adaptation

Neural adaptation has been frequently observed at multiple levels along the central auditory pathway (Harms et al., 2016) including the AC (Taaseh et al., 2011; Ulanovsky et al., 2003, 2004). Given the highly hierarchical and interactive organization of the auditory system, it is still under debate whether the observed cortical adaptation is inherited from the already adapted subcortical inputs, whether it is locally generated within the cortex and then further projected back to influence the subcortical adaptation through the corticofugal system, or whether it involves both subcortical and cortical contributions. Several studies have addressed the functional role of the sensory cortex in contributing to adaptation. Ulanovsky et al. (2003) reported A1 neurons of cats exhibiting SSA, whereas the thalamic neurons were insensitive towards the statistics of stimulation; therefore the authors suggested an intracortical generator of SSA. Natan et al. (2015) reported two types of interneurons in the A1 of mice differentially contributing to adaptation of standard and deviants in SSA. Specifically, the parvalbumin-positive interneurons perform equal inhibition towards standard and deviant stimuli, whereas the somatostatin-positive interneurons selectively reduce the excitatory response towards standards but not the deviants. Moreover, it has been observed that along the lemniscal pathway, SSA first shows up in the AC, whereas along the non-lemniscal pathway, the prevailing presence of SSA is seen all along it and as early at the IC (Carbajal & Malmierca, 2018). Carbajal and Malmierca claim that the observation of SSA in the lemniscal field of the AC, namely the A1, demonstrates the cortical contribution to SSA, while assuming that the A1 receives merely lemniscal inputs. However, anatomical research (Saldeitis et al., 2014) has demonstrated that the A1 is receiving a mixture of inputs from both pathways. It is thus not that straight forward to determine whether adaptation in the A1 is inherited from the subcortical stations through the non-lemniscal pathway or at least partly generated cortically.

In the current study, despite not distinguishing the lemniscal and non-lemniscal inputs into the cortex and their individual development intracortically, I examined the potential influence of the intracortical processing on the cortical RS as an intact factor. This goal was achieved via cortical silencing with muscimol combined with CSD analysis—providing assessment of the cortical response at a layer-specific resolution. Together with Fi, they jointly enabled a straight forward comparison of the RS kinetics between untreated and muscimol states as well as

between cortical layers.

Szymanski et al., (2009) is one of a few studies that addressed the cortical layer-specificity of auditory adaptation using CSD analysis. They reported that using an oddball paradigm with an SOI of 0.3 s, more pronounced SSA was observed in the infragranular layer than in the granular layer of the anesthetized rat AC, i.e., stronger SSA was measured by a SSA index comparing the response level towards the same tone being standard and being deviant. This result is in line with my results of the layer-specific repetition suppression index (RSI) across SOIs. At the shortest two SOI values of 0.219 s and 0.328 s, the infragranular RSI is clearly lower than the granular RSI that indicated a stronger infragranular RS. Moreover, their layer-specific SSA level can be largely explained by the current layer-specific kinetics of RS characterized by the time constants. Specifically, granular layer exhibited shorter τ_{gran} at around 0.3 s than τ_{infra} at around 0.5 s. This means that the lifetime of RS is longer in infragranular than in granular layers, which means that the peak amplitude of the infragranular sink was more strongly suppressed at shorter SOIs and needed longer SOIs to recover to its saturation level.

Szymanski et al., (2009) interpreted the stronger infragranular adaptation as a pure outcome of intracortical processing. They based their interpretation on a simplified assumption that the infragranular adaptation is merely triggered by the intracortical projection from the granular layer. However, while cortical silencing, I observed the appearance of RS at the very initial activation of both the granular and infragranular sink, which implies RS inputs originating from the thalamocortical synapse. Notably, the time constant became equal between granular and infragranular layers after removing the cortical processing, with a prolonged granular time constant and an unchanged infragranular time constant compared to the untreated state with cortical processing. These equal RS kinetics in both thalamocortical recipient layers cannot be explained, at least solely, by the unbalanced lemniscal and non-lemniscal inputs into both layers (Saldeitis et al., 2014), otherwise they would show different kinetics. However, my results can be well explained by the work by Chung et al. (2002), who demonstrated *in vivo* for the first time that the short-term synaptic depression of thalamocortical synapses is the main cause of RS in the rat somatosensory cortex. Soon afterwards, Best and Wilson (2004) also suggested that the short-term synaptic depression of cortical afferent synapse may contribute to olfactory cortical adaptation in rats.

Moreover, although Szymanski et al. (2009) also applied CSD analysis to determine the layer

specific response, they computed the RMS of the layer-specific CSD across a time window of 150 ms after tone onset as an overall response measure used for calculating the SSA index. Therefore, their response measure includes all of the sink and source activations occurring in during that relatively long time interval. Szymansiki's cortical activation measure might therefore also include source activities reflecting return currents driven by synapses in neighboring layers. Clearly, the response measures used in my study are much more layer- and sink-specific, and less confounded by ongoing sources and sinks of neighboring layers.

4.3 Potential mechanisms underlying cortical repetition suppression

Previous studies have shown that within the neocortex, at the level of spiking and membrane potentials, the dependence of the adaptation level on stimulus statistics—including stimulus intervals, proportion of deviants, and frequency distance between deviant and standard—can be attributed to multiple response mechanisms. Operating over multiple timescales (Latimer et al., 2019; Ulanovsky et al., 2004), adaptation was thereby suggested to serve as effective coding of natural stimuli that appear over a wide temporal and acoustic range. Along a train of repetitive stimuli, the response gradually decays until reaching a steady state. This steady state of RS, which is the focus of the current study, is determined by the balance between the stimulus-induced suppression and SOI-allowed recovery. At this balanced state, the influences of statistical non-stationarities and transients on adaptation were strongly reduced. The SOI dependence of the steady state of RS can be largely explained by a simple exponential function with single time constant τ. The estimated time constant characterizes the lifetime of the RS. Such an exponential fitting approach has been previously studied on a macroscopic level with EEG and MEG (Lü et al., 1992; Lu et al., 1992; Zacharias et al., 2012). Theoretical studies further suggest that the exponential relation between steady state RS and SOI can be attributed to local synaptic depression in concert with large-scale networking that might serve as a linear low pass filter (May et al., 2015).

Muscimol inhibits intracortical processing while leaving intact the activation of the thalamocortical recipient neurons and the their input to the cortex via thalamocortical synapses (Deane et al., 2020; Happel et al., 2010). The prolonged τ_{gran} at the muscimol state strongly suggests the dependence of the short-lived granular RS kinetics on intracortical inputs, whereas the barely affected τ_{infra} suggest that the infragranular adaptation did not depend on the

intracortical inputs. Thereby, the corticocortical processing shortened the lifetime of RS in the granular layer after receiving the more adapted thalamocortical inputs. Fishman and Steinschneider (2012) investigated deviant response via CSD measures in the A1 of awake macaque monkeys. Their results revealed more prominent differences between deviant and standard responses in the later part of the initial supragranular current sink activity, rather than the early part. Therefore, they suggested that intracortical processing enhanced SSA originating from subcortical levels. This is in accordance with Szymanski et al. (2009) who concluded intracortical strengthening of SSA. Via intracellular recordings in the rat A1 and cortical silencing by muscimol, Liu et al. (2007) revealed that although the thalamocortical input defines the range of the receptive field of the cortical response, the weakly tuned thalamocortical input showing a rather flat tuning curve is significantly sharpened by the intracortical processing. The similar range but different sharpness of thalamocortical and intracortical tunings imply a recurrent circuitry in which local, similarly-tuned neurons excite each other. In the current FR measurements, similarly: initial, granular, near-BF responses were amplified relative to initial, simultaneous, infragranular responses, while muscimol flattened out the difference in near-BF amplification between granular and infragranular layers. Such a cortical gain modulation might play an important role in boosting up and accelerating the already stronger adapted thalamocortical inputs into the granular layer. Selective gain amplification in granular layers could therefore attenuate RS levels of the afferent inputs originating from the depression of thalamocortical synapses.

Given the different response strengths due to layer difference, condition differences might have caused biases in the estimation of time constant τ. Correlation analysis showed that the observed significant differences in time constants across layers and conditions were a genuine layer effects, which cannot be simply explained by differences in the saturation amplitudes between layers. Moreover, each τ was deduced from an exponential fitting to the SOI dependent response levels, which can be seen as a normalization within each fitting event, regardless of the individual saturation amplitude. In answering the question whether the SSA is merely a result of the response strength varying along the tuning curve as a function of stimulus frequency, Taaseh et al. (2011) has also shown that SSA was not dependent on response strength alone. SSA was prominent at a narrower frequency distance range than the tuning width of LFP.

The comparison of time constants of the sink peaks and total current yielded further insight into the potential mechanism causing the intracortical shortening of the time constant τ for the sink peak in the granular layer. Time constants derived from the total current were shorter in both layers and all conditions than the corresponding τ values derived from sink peaks, which reflect weaker RS in the total sink current flow. Moreover, the effect of the cortical shortening the time constant τ in the granular layer was weaker for the total current than for the sink peak. The sink peak depends not only on the amount, but also on the maximum coincidence of the synaptic events at the time point of peak latency, whereas the peak integral depends on the total amount of the synaptic events during the sink activation. This demonstrates the important role of synchronization of intracortical synaptic events in shaping the cortical RS. Thus, the cortical RS in general as well as the cortical shortening of the RS in the granular layer were dependent on the synchronization of intracortical synaptic events. These results are in accordance with the findings by Hershenhoren et al. (2014) that the SSA was more pronounced in the spiking responses—which also reflects the coincidence and synchronization of synaptic events—than at the level of membrane potential. They interpreted this effect as a consequence of the nonlinear transformation between membrane potential to spike activity.

Time constants were deduced from sink-specific measures (sink activation and sink integral) within early granular and infragranular layers. However, further correlation analysis illustrated how the fast and slow kinetics appeared in the early sinks evolved across layers with increasing latency. During cortical processing, early activation in CSD profiles show higher correlation with fast RS kinetics in the granular layer and with slow kinetics in infragranular layer; and later the fast kinetics gradually spreads down to the infragranular layer. However, cortical silencing removed the layer specificity and both layers revealed slow RS kinetics, even during initial activation in granular layers. This confirmed what has been previously discussed: that both thalamocortical recipient layers inherited RS from thalamocortical synapses with similar slow kinetics. Then intracortical processing actively accelerate the slow kinetics resulting in a fast kinetics which is then projected downwards to the infragranular layers. Such an intracortical processing that amplifies SSA originating from subcortical levels was also suggested by Fishman and Steinschneider (2012).

Although the focus of the current study is to compare the kinetics of RS in granular and infragranular layers, cortical processing in these layers are not independent from each other.

Instead, layer activations coexist and interact in a larger network, including the cortico-thalamo-cortical feedback loops that also contribute to the synchronization of cortical activity (Timofeev et al., 2013). The local synchronization of synaptic interactions has been suggested as responsible for generating local field potentials (Timofeev et al., 2013). Both layers receive thalamocortical inputs, then cortical processing spreads from the granular layer simultaneously upwards to the supragranular layer and downwards to the infragranular layer (Happel et al., 2010; Szymanski et al., 2009). As the known output layer, the infragranular layer sends cortical feedback down to the subcortical centers through the corticofugal (descending) system. Research has indicated that the corticofugal system plays a role in adjusting and improving subcortical signal processing according to the auditory experience, sharpening tuning and gain control, and acting on both short-term changes and long-term plasticity (He, 2003; Suga et al., 2000; Winer, 2005; Yan et al., 2005; Yu et al., 2004). The influences of the cortical SSA (Ulanovsky et al., 2003, 2004) on SSA in the vMGB through corticofugal control was demonstrated for the first time by Bäuerle et al. (2011), in the anesthetized Mongolian gerbil. They observed SSA in the vMGB as part of the lemniscal pathway, where SSA was usually either not detected (Ulanovsky et al., 2003, 2004) or just shown to a very limited degree (Anderson et al., 2009; Antunes et al., 2010). However, the cortical inactivation with muscimol largely removed the SSA measured by the deviant-standard difference in the vMGB. This observation led to the conclusion that the AC is influencing the generation of SSA of the auditory thalamus. Through such influence, the cortex would be able to adjust its own inputs through corticofugal control. Therefore, through continuous and interactive communication, auditory centers, as well as their subdivisions along both of the ascending and descending pathways, are responsible for shaping the gating and processing of auditory information of each other and themselves.

4.4 Conclusion

Cortical adaptation has been explained by multiple mechanisms. It has been suggested to be inherited from subcortical sensory pathways, to rely on synaptic depression of the thalamocortical synapse, to be influenced by intracortical balance between excitation and inhibition, and to be modulated by recurrent corticoefferent feedback. In this doctoral project, the goal was to disentangle intracortical from subcortical contributions to cortical adaptation within this hierarchical network. I have investigated RS as a fundamental aspect of adaptation,

and systematically varied SOIs to create steady state adaptation at different strengths. Layer-specific analysis of synaptic mass inputs was performed using CSD analysis in the primary auditory cortex of anesthetized gerbils. To study the effect of intracortical synaptic input to adaptation, the intracortical processing was silenced with the $GABA_A$-agonist muscimol.

In summary, the major finding of my study shows that initial granular and infragranular sinks display differing RS kinetics. The lifetime of the RS in the infragranular sink was nearly twice as long as that of the granular sink. After pharmacologically silencing the intracortical processing, the lifetime of RS in both layers became comparable with a prolonged time constant in granular layer and an unchanged time constant in the infragranular layer. These demonstrate an intracortical contribution to RS in the granular layer and it raises the implication of an intracortical mechanism that re-accelerates the suppressed thalamocortical inputs, therefore effectively reducing the local time constant of the RS kinetics. Furthermore, for the first time, it was shown that RS was stronger for the sink peak than for the total current, indicating an important role of synchronization of synaptic events in RS.

4.5 Perspectives and outlook

This doctoral project was undertaken to pursue further understanding of the cortical role in processing auditory adaptation via disentangling the different sub- and intracortical contributions on a circuitry level. The results demonstrate that the intracortical circuitry can shape auditory adaptation in a layer-specific manner. However, the exact cortical mechanisms that lead to these effects is still unknown. It might require feedforward synaptic excitation and/or intracortical recurrent excitation. The observed role of synchronization of synaptic events further suggests the involvement of a certain nonlinear transformation (Hershenhoren et al., 2014) between various scales of neuronal activity, i.e. membrane potential, spike activity, LFP, and so on.

While the current study differentiated thalamocortical from intracortical contributions to adaptation in the prominent current sinks, it did not separate different input streams like lemniscal and non-lemniscal inputs. As previously discussed by Carbajal and Malmierca (2018), neurons consisting in the lemniscal nucleus are sharply tuned and perform rather precise and ascending coding of the physical features of the sound up to the cortex, whereas non-lemniscal divisions perform their own processing of the received inputs and form a loop-like connectivity

network including both ascending and descending projections. Together with the current findings of cortical processing of the adaptation, whether those parallel streams undergo individual intracortical shaping and how the corticofugal projections distinguishingly influence each ascending stream in the following information coding are the next interesting questions, which would require cell-specific research tools like optogenetics with a combination of simultaneous recording within multiple centers.

The ultimate goal of gaining knowledge of neural adaptation during anesthesia is to better understand how it serves the perception and decision making of a behaving individual, and, in the end, enhance the chance of survival and reproduction. In the awake behaving animal, SSA has been found to be shaped by experience (Yaron et al., 2020). Specifically, the level of SSA measured by the contrast between standard and deviant responses, was changing in a way that depends on the behavioral relevance of the presented tone. Behavioral evidences by Zempeltzi et al. (2020) have shown that motor-related stimuli were reflected in a layer-specific manner in the CSD profile. During a detection learning task, where all the auditory stimuli are associated with a motor action as the correct response, the auditory cortical responses reflect initiation of motor actions prominently in deeper cortical layers. Future work could attempt to gain insights into the behavioral relevance of the cortical shaping of RS, namely whether and how the intracortical acceleration of fast RS kinetics would potentially serve the motor action through the corticofugal system; whether the cortical shaping of granular RS kinetics depends on the state of the animal (e.g. awake or anesthetized or behaving); whether attenuation of the auditory response plays a role in avoidance learning via serving behavior inhibition. One hypothesis would be that stronger adaptation in the infragranular layer might support blocking the execution of a responding movement via holding the information for processing and future guiding of the behavior.

Another potentially interesting research area is the developmental perspectives of auditory adaptation. Evidence has shown that during postnatal stages, intracortical circuits undergo rapid developmental maturation, including refining the tonotopic map in A1. Sun et al. (2019) found that during development, although the frequency tuning of thalamic output remained unchanged, the tuning curve became sharpened for both thalamocortical and intracortical excitatory inputs to the granular layer. In recent decades, the application of RS paradigm in adult and developmental cognitive neuroscience has been gaining attraction due to it allowing easy

comparison across ages and measurement technologies without requiring behavioral learning (Nordt et al., 2016). Taking those findings into account, using the experimental approach applied in my study, one could potentially shed light on developmental cognitive functions using animal subjects allowing for the investigation of underlying intracortical mechanisms.

Appendix

A.1 Results – Supplementary information

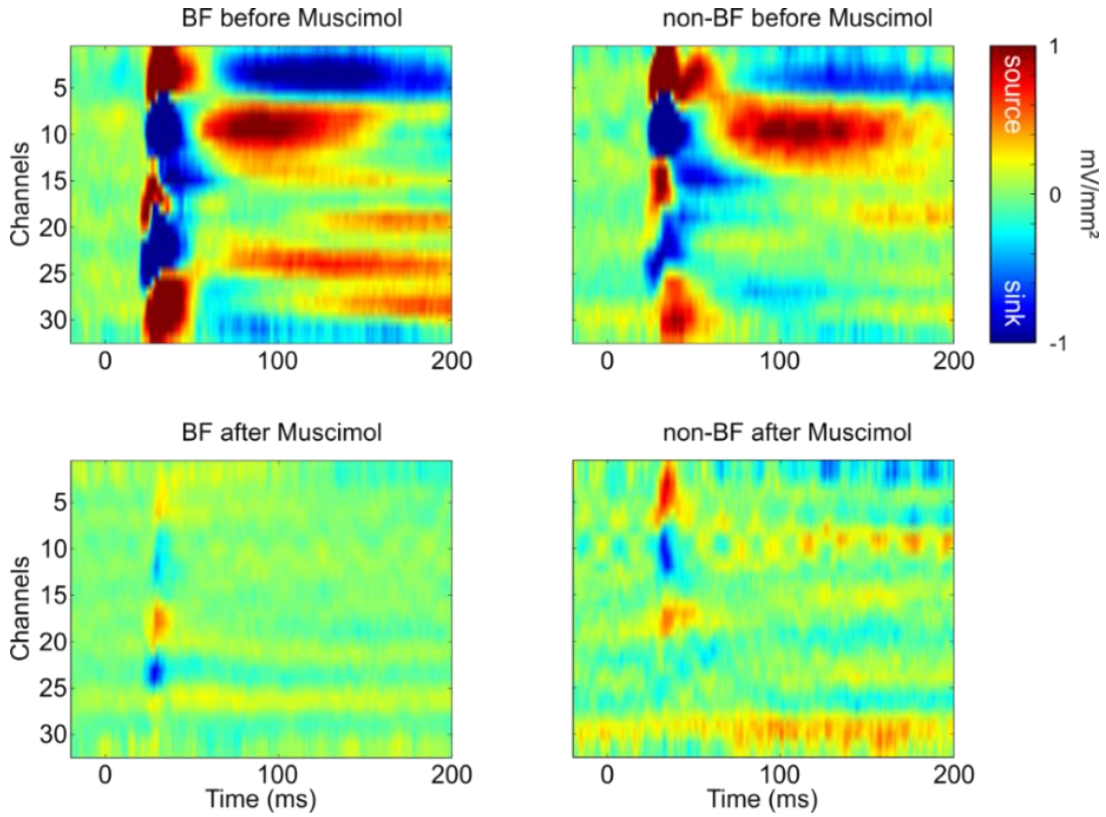

Figure A.1. 1 Example of pure tone evoked CSD profiles (*Single subject*)

A.2 Tables

Animal	*Color code*	*BF [kHz]*	*Non-BF [kHz]*
a001		1	0.25
a002		1	4
a003		1	4
a004		4	1
a005		1	4
a006		4	1
a007		2	0.5
a008		2	0.5
a009		1	4

Table A.2. 1 Presented BF and non-BF for each subject

Trial structure		
SOI (s)	Tone-sequence duration (s)	Saturated/ total tone repetitions in each trial
0.219	7.2	24/33
0.328	7.2	16/22
0.438	7.2	13/17
0.656	7.2	8/11
0.875	7.2	7/9
1.313	7.2	5/6
1.75	7.2	4/5
2.626	14.2	5/6
3.5	14.2	4/5
7	14.2	2/3

Table A.2. 2 Detailed information of trial structure for each SOI

Bibliography

Anderson, L. A., Christianson, G. B., Linden, J. F. (2009). Stimulus-Specific Adaptation Occurs in the Auditory Thalamus. *Journal of Neuroscience*, *29*(22), 7359–7363.

Antunes, F. M., Nelken, I., Covey, E., Malmierca, M. S. (2010). Stimulus-Specific Adaptation in the Auditory Thalamus of the Anesthetized Rat. *PLoS ONE*, *5*(11), e14071.

Auksztulewicz, R., Friston, K. (2016). Repetition suppression and its contextual determinants in predictive coding. *Cortex*, *80*, 125–140.

Bäuerle, P., von der Behrens, W., Kössl, M., Gaese, B. H. (2011). Stimulus-specific adaptation in the gerbil primary auditory thalamus is the result of a fast frequency-specific habituation and is regulated by the corticofugal system. *Journal of Neuroscience*, *31*(26), 9708–9722.

Best, A. R., Wilson, D. A. (2004). Coordinate Synaptic Mechanisms Contributing to Olfactory Cortical Adaptation. *Journal of Neuroscience*, *24*(3), 652–660.

Brunk, M. G. K., Deane, K. E., Kisse, M., Deliano, M., Vieweg, S., Ohl, F. W., Lippert, M. T., Happel, M. F. K. (2019). Optogenetic stimulation of the VTA modulates a frequency-specific gain of thalamocortical inputs in infragranular layers of the auditory cortex. *Scientific Reports*, *9*(1), 20385.

Budinger, E., Heil, P., Scheich, H. (2000). Functional organization of auditory cortex in the Mongolian gerbil (Meriones unguiculatus). III. Anatomical subdivisions and corticocortical connections. *The European Journal of Neuroscience*, *12*(7), 2425–2451.

Bujas, Z., Ajduković, D., Szabo, S., Mayer, D., Vodanović, M. (1995). Central processes in gustatory adaptation. *Physiology & Behavior*, *57*(5), 875–880.

Buzsáki, G., Anastassiou, C. A., Koch, C. (2012). The origin of extracellular fields and currents-EEG, ECoG, LFP and spikes. *Nature Reviews Neuroscience*, *13*(6), 407–420.

Carbajal, G. V., Malmierca, M. S. (2018). The unique role of the non-lemniscal pathway on stimulus-specific adaptation (SSA) in the auditory system. *Proceedings of the International Symposium on Auditory and Audiological Research*, *6*(February), 95–106.

Chung, S., Li, X., Nelson, S. B. (2002). Short-term depression at thalamocortical synapses contributes to rapid adaptation of cortical sensory responses in vivo. *Neuron*, 34(3), 437-446.

Davison, A. C., Hinkley, D. V. (1997). Bootstrap Methods and their Application. In *Cambridge Series in Statistical and Probabilistic Mathematics*. Cambridge University Press.

Deane, K. E., Brunk, M. G. K., Curran, A. W., Zempeltzi, M. M., Ma, J., Lin, X., Abela, F., Aksit, S., Deliano,

M., Ohl, F. W., Happel, M. F. K. (2020). Ketamine anaesthesia induces gain enhancement via recurrent excitation in granular input layers of the auditory cortex. *The Journal of Physiology*, *598*(13), 2741–2755.

DiCiccio, T. J., Efron, B. (1996). Bootstrap Confidence Intervals. *Statistical Science*, *11*(3), 189–212.

Duque, D., Pérez-González, D., Ayala, Y. A., Palmer, A. R., Malmierca, M. S. (2012). Topographic distribution, frequency, and intensity dependence of stimulus-specific adaptation in the inferior colliculus of the rat. *Journal of Neuroscience*, *32*(49), 17762–17774.

Edeline, J.M., Hars, B., Hennevin, E., Cotillon, N. (2002). Muscimol Diffusion after Intracerebral Microinjections: A Reevaluation Based on Electrophysiological and Autoradiographic Quantifications. *Neurobiology of Learning and Memory*, *78*(1), 100–124.

Efron, B. (1979). Bootstrap Methods: Another Look at the Jackknife. *The Annals of Statistics*, *7*(1), 1–26.

Festing, M. F. W., Altman, D. G. (2002). Guidelines for the design and statistical analysis of experiments using laboratory animals. *ILAR Journal*, *43*(4), 244–257.

Fishman, Y. I., Steinschneider, M. (2012). Searching for the mismatch negativity in primary auditory cortex of the awake monkey: Deviance detection or stimulus specific adaptation? *Journal of Neuroscience*, *32*(45), 15747–15758.

Fitzgerald, K., Todd, J. (2020). Making Sense of Mismatch Negativity. *Frontiers in Psychiatry*, *11*(June), 1–19.

Fong, C. Y., Law, W. H. C., Uka, T., Koike, S. (2020). Auditory Mismatch Negativity Under Predictive Coding Framework and Its Role in Psychotic Disorders. In *Frontiers in Psychiatry*, 11, 557932.

Franco, N. H., Olsson, I. A. S. (2014). Scientists and the 3Rs: attitudes to animal use in biomedical research and the effect. *Laboratory Animals*, *48*(1), 50–60.

Garrido, M. I., Kilner, J. M., Kiebel, S. J., Stephan, K. E., Baldeweg, T., Friston, K. J. (2009). Repetition suppression and plasticity in the human brain. *NeuroImage*, *48*(1), 269–279.

Gibson, B. Y. J. J. (2004). *Gibson (1937) Adaptation, After-Effect, and Contrast in the Perception of Tilted Lines. Ii. Simultaneous Contrast and the Areal Restriction of the After-Effect*. 1–17.

Goodhue, D. L., Lewis, W., Thompson, R. (2012). Does PLS Have Advantages for Small Sample Size or Non-Normal Data? *MIS Quarterly*, *36*(3), 981–1001.

Groppe, D., Urbach, T., Kutas, M. (2011). Mass univariate analysis of event-related brain potentials/fields I: A critical tutorial review. *Psychophysiology*, *48*, 1711–1725.

Grundy, D. (2015). Principles and standards for reporting animal experiments in The Journal of Physiology and Experimental Physiology. *Journal of Physiology*, *593*(12), 2547–2549.

Happel, Max F.K., Deliano, M., Handschuh, J., Ohl, F. W. (2014). Dopamine-Modulated Recurrent Corticoefferent Feedback in Primary Sensory Cortex Promotes Detection of Behaviorally Relevant Stimuli. *Journal of Neuroscience*, *34*(4), 1234–1247.

Happel, Max F.K., Jeschke, M., Ohl, F. W. (2010). Spectral Integration in Primary Auditory Cortex Attributable to Temporally Precise Convergence of Thalamocortical and Intracortical Input. *Journal of Neuroscience*, *30*(33), 11114–11127.

Harms, L., Michie, P. T., Näätänen, R. (2016). Criteria for determining whether mismatch responses exist in animal models: Focus on rodents. *Biological Psychology*, *116*, 28–35.

He, J. (2003). Corticofugal modulation of the auditory thalamus. *Experimental Brain Research*, *153*(4), 579–590.

Hershenhoren, I., Taaseh, N., Antunes, F. M., Nelken, I. (2014). Intracellular correlates of stimulus-specific adaptation. *Journal of Neuroscience*, *34*(9), 3303–3319.

Javit, D. C., Steinschneider, M., Schroeder, C. E., Vaughan, H. G., Arezzo, J. C. (1994). Detection of stimulus deviance within primate primary auditory cortex: intracortical mechanisms of mismatch negativity (MMN) generation. *Brain Research*, *667*(2), 192–200.

Köster, E. P., de Wijk, R. A. (1991). *Olfactory Adaptation BT - The Human Sense of Smell*, 199–215.

Krantz, J. (2012). What is Sensation and Perception? *Experiencing Sensation & Perception*, 1–20.

Kujala, T., Näätänen, R. (2001). The mismatch negativity in evaluating central auditory dysfunction in dyslexia. *Neuroscience and Biobehavioral Reviews*, *25*(6), 535–543.

Latimer, K. W., Barbera, X. D., Sokoletsky, M., Awwad, B., Katz, X. Y., Nelken, X. I., Lampl, X. I., Fairhall, A. L., Priebe, N. J. (2019). *Multiple Timescales Account for Adaptive Responses across Sensory Cortices, 39*(50), 10019–10033.

Liu, B. H., Wu, G. K., Arbuckle, R., Tao, H. W., Zhang, L. I. (2007). Defining cortical frequency tuning with recurrent excitatory circuitry. *Nature Neuroscience*, *10*(12), 1594–1600.

Lu, K., Vicario, D. S. (2011). Toward a neurobiology of auditory object perception: What can we learn from the songbird forebrain? *Current Zoology*, *57*(6), 671–683.

Lu, Z. L., Williamson, S. J., Kaufman, L. (1992). Behavioral lifetime of human auditory sensory memory predicted by physiological measures. *Science*, *258*(5088), 1668–1670.

Lü, Z., Williamson, S. J., Kaufman, L. (1992). Human auditory primary and association cortex have differing lifetimes for activation traces. *In Brain Research*, 572(1–2), 236–241.

Malmierca, M. S., Anderson, L. A., Antunes, F. M. (2015). The cortical modulation of stimulus-specific adaptation in the auditory midbrain and thalamus: A potential neuronal correlate for predictive coding. *Frontiers in Systems Neuroscience*, *9*(MAR), 1–14.

Malmierca, M. S., Cristaudo, S., Pérez-González, D., Covey, E. (2009). Stimulus-specific adaptation in the inferior colliculus of the anesthetized rat. *Journal of Neuroscience*, *29*(17), 5483–5493.

Malmierca, M. S., Sanchez-Vives, M. V., Escera, C., Bendixen, A. (2014). Neuronal adaptation, novelty detection and regularity encoding in audition. *Frontiers in Systems Neuroscience*, *8*(JUNE), 1–9.

May, P. J. C., Tiitinen, H. (2010). Mismatch negativity (MMN), the deviance-elicited auditory deflection, explained. *Psychophysiology*, *47*(1), 66–122.

May, P. J. C., Westö, J., Tiitinen, H. (2015). Computational modelling suggests that temporal integration results from synaptic adaptation in auditory cortex. *European Journal of Neuroscience*, *41*(5), 615–630.

May, P., Tiitinen, H. (2001). Human cortical processing of auditory events over time. *Neuroreport*, *12*(3), 573–577.

Mayrhauser, L., Bergmann, J., Crone, J., Kronbichler, M. (2014). Neural repetition suppression: Evidence for perceptual expectation in object-selective regions. *Frontiers in Human Neuroscience*, *8*(1 APR), 1–8.

Michie, P. T., Malmierca, M. S., Harms, L., Todd, J. (2016a). The neurobiology of MMN and implications for schizophrenia. *Biological Psychology*, *116*, 90–97.

Michie, P. T., Malmierca, M. S., Harms, L., Todd, J. (2016b). Understanding the neurobiology of MMN and its reduction in schizophrenia. *Biological Psychology*, *116*, 1–3.

Mitzdorf, U. (1985). Current source-density method and application in cat cerebral cortex: investigation of evoked potentials and EEG phenomena. *Physiological Reviews*, *65*(1), 37–100.

Näätänen, R., Gaillard, A. W. K., Mäntysalo, S. (1978). Early selective-attention effect on evoked potential reinterpreted. *Acta Psychologica*, *42*(4), 313–329.

Näätänen, R., Kujala, T., Escera, C., Baldeweg, T., Kreegipuu, K., Carlson, S., Ponton, C. (2012). The mismatch negativity (MMN) – A unique window to disturbed central auditory processing in ageing and different clinical conditions. *Clinical Neurophysiology*, *123*(3), 424–458.

Näätänen, R., Paavilainen, P., Rinne, T., Alho, K. (2007). The mismatch negativity (MMN) in basic research of central auditory processing: A review. *Clinical Neurophysiology*, *118*(12), 2544–2590.

Natan, R. G., Briguglio, J. J., Mwilambwe-Tshilobo, L., Jones, S. I., Aizenberg, M., Goldberg, E. M., Geffen, M. N. (2015). Complementary control of sensory adaptation by two types of cortical interneurons. *ELife*, *4*(2015).

Natan, R. G., Rao, W., Geffen, M. N. (2017). Cortical Interneurons Differentially Shape Frequency Tuning following Adaptation. *Cell Reports*, *21*(4), 878–890.

Nelken, I. (2004). Processing of complex stimuli and natural scenes in the auditory cortex. In *Current Opinion in Neurobiology* 14(4), 474–480.

Nelken, I. (2014). Stimulus-specific adaptation and deviance detection in the auditory system: experiments and models. In *Biological Cybernetics* 108(5), 655-663.

Nelken, I., Ulanovsky, N. (2007). Mismatch negativity and stimulus-specific adaptation in animal models. In *Journal of Psychophysiology* 21(3–4), 214–223.

Nordt, M., Hoehl, S., Weigelt, S. (2016). The use of repetition suppression paradigms in developmental cognitive neuroscience. *Cortex*, *80*, 61–75.

Ohl, Frank W., Scheich, H., Freeman, W. J. (2000). Topographic analysis of epidural pure-tone-evoked potentials in gerbil auditory cortex. *Journal of Neurophysiology*, *83*(5), 3123–3132.

Ohl, Frank W., Wetzel, W., Wagner, T., Rech, A., Scheich, H. (1999). Bilateral ablation of auditory cortex in Mongolian gerbil affects discrimination of frequency modulated tones but not of pure tones. *Learning and Memory*, *6*(4), 347–362.

Otto, G., Jrge, S. (2012). The Mongolian Gerbil as a Model for the Analysis of Peripheral and Central Age-Dependent Hearing Loss.

Pazo-Alvarez, P., Cadaveira, F., Amenedo, E. (2003). MMN in the visual modality: a review. *Biological Psychology*, *63*(3), 199–236.

Pérez-González, D., Malmierca, M. S. (2014). Adaptation in the auditory system: an overview. *Frontiers in Integrative Neuroscience*, *8*(FEB), 1–10.

Pérez-González, D., Malmierca, M. S., Covey, E. (2005). Novelty detector neurons in the mammalian auditory midbrain. *European Journal of Neuroscience*, *22*(11), 2879–2885.

Phelps, S. M. (2007). Sensory ecology and perceptual allocation: New prospects for neural networks. *Philosophical Transactions of the Royal Society B: Biological Sciences*, *362*(1479), 355–367.

Puccini, G. D., Sanchez-Vives, M. V, Compte, A. (2006). Selective detection of abrupt input changes by integration of spike-frequency adaptation and synaptic depression in a computational network

model. *Journal of Physiology-Paris*, *100*(1), 1–15.

Rabinowitz, N. C., Willmore, B. D. B., Schnupp, J. W. H., King, A. J. (2011). Contrast gain control in auditory cortex. *Neuron*, *70*(6), 1178–1191.

Ryan, A. (1976). Hearing sensitivity of the mongolian gerbil, Meriones unguiculatis. *The Journal of the Acoustical Society of America*, *59*(5), 1222–1226.

Saldeitis, K., Happel, M. F. K., Ohl, F. W., Scheich, H., Budinger, E. (2014). *Anatomy of the Auditory Thalamocortical System in the Mongolian gerbil : Nuclear Origins and Cortical*. *2430*, 2397–2430.

Sarro, E. C., Sanes, D. H. (2010). Prolonged maturation of auditory perception and learning in gerbils. *Developmental Neurobiology*, *70*(9), 636–648.

Scheich, H., Brechmann, A., Brosch, M., Budinger, E., Ohl, F. W. (2007a). The cognitive auditory cortex: Task-specificity of stimulus representations. *Hearing Research*, *229*(1), 213–224.

Scheich, H., Brechmann, A., Brosch, M., Budinger, E., Ohl, F. W. (2007b). The cognitive auditory cortex: Task-specificity of stimulus representations. *Hearing Research*, *229*(1–2), 213–224.

Somani, S., Shukla, J. (2012). Research & reviews : journal of medical and health sciences. *Research & Reviews: Journal of Medical and Health Sciences*, *3*(4), 33–42.

Squires, N. K., Squires, K. C., Hillyard, S. A. (1975). Two varieties of long-latency positive waves evoked by unpredictable auditory stimuli in man. *Electroencephalography and Clinical Neurophysiology*, *38*(4), 387–401.

Suga, N., Gao, E., Zhang, Y., Ma, X., Olsen, J. F. (2000). The corticofugal system for hearing: Recent progress. *Proceedings of the National Academy of Sciences of the United States of America*, *97*(22), 11807–11814.

Sun, Y. J., Liu, B. H., Tao, H. W., Zhang, L. I. (2019). Selective strengthening of intracortical excitatory input leads to receptive field refinement during auditory cortical development. *Journal of Neuroscience*, *39*(7), 1195–1205.

Szymanski, F. D., Garcia-Lazaro, J. A., Schnupp, J. W. H. H. (2009). Current source density profiles of stimulus-specific adaptation in rat auditory cortex. *Journal of Neurophysiology*, *102*(3), 1483–1490.

Taaseh, N., Yaron, A., Nelken, I. (2011). Stimulus-Specific Adaptation and Deviance Detection in the Rat Auditory Cortex. *PLoS ONE*, *6*(8), e23369.

Tervaniemi, M. (2001). Musical sound processing in the human brain evidence from electric and magnetic recordings. *Annals of the New York Academy of Sciences*, *930*, 259–272.

Thomas, H., Tillein, J., Heil, P., Scheich, H. (1993). Functional Organization of Auditory Cortex in the Mongolian Gerbil (Meriones unguiculatus). I. Electrophysiological Mapping of Frequency Representation and Distinction of Fields. *European Journal of Neuroscience*, *5*(7), 882–897.

Timofeev, I., Bazhenov, M., Seigneur, J., Sejnowski, T. (2013). Neuronal Synchronization and Thalamocortical Rhythms during Sleep, Wake, and Epilepsy. *Jasper's Basic Mechanisms of the Epilepsies*, 157–175.

Ulanovsky, N., Las, L., Farkas, D., Nelken, I. (2004). Multiple time scales of adaptation in auditory cortex neurons. *Journal of Neuroscience*, *24*(46), 10440–10453.

Ulanovsky, N., Las, L., Nelken, I. (2003). Processing of low-probability sounds by cortical neurons. *Nature Neuroscience*, *6*(4), 391–398.

Umbricht, D., Vyssotki, D., Latanov, A., Nitsch, R., Lipp, H.-P. (2005). Deviance-related electrophysiological activity in mice: is there mismatch negativity in mice? *Clinical Neurophysiology*, *116*(2), 353–363.

Utzerath, C., St John-Saaltink, E., Buitelaar, J., De Lange, F. P. (2017). Repetition suppression to objects is modulated by stimulus-specific expectations. *Scientific Reports*, *7*(1), 1–8.

von der Behrens, W., Bäuerle, P., Kössl, M., Gaese, B. H. (2009). Correlating stimulus-specific adaptation of cortical neurons and local field potentials in the awake rat. *Journal of Neuroscience*, *29*(44), 13837–13849.

Wark, B., Lundstrom, B. N., Fairhall, A. (2007). Sensory adaptation. *Current Opinion in Neurobiology*, *17*(4), 423–429.

Webster, M. A. (2012). Evolving concepts of sensory adaptation. *F1000 Biology Reports*, *4*(1), 1–7.

Wetzel, W., Wagner, T., Ohl, F. W., Scheich, H. (1998). Categorical discrimination of direction in frequency-modulated tones by Mongolian gerbils. *Behavioural Brain Research*, *91*(1), 29–39.

Winer, J. A. (2005). Decoding the auditory corticofugal systems. *Hearing Research*, *207*(1–2), 1–9.

Winer, J. A., Schreiner, C. E. (2005). The central auditory system: A functional analysis. *In The Inferior Colliculus* (Issue January 2005).

Winkler, I., Denham, S. L., Nelken, I. (2009). Modeling the auditory scene: predictive regularity representations and perceptual objects. In *Trends in Cognitive Sciences,* 13(12), 532–540.

Wrobel, C., Dieter, A., Huet, A., Keppeler, D., Duque-Afonso, C. J., Vogl, C., Hoch, G., Jeschke, M., Moser, T. (2018). Optogenetic stimulation of cochlear neurons activates the auditory pathway and restores auditory-driven behavior in deaf adult gerbils. *Science Translational Medicine*, *10*(449), eaao0540.

Yamauchi, T., Hori, T., Takahashi, T. (2000). Presynaptic inhibition by muscimol through GABAB receptors. *The European Journal of Neuroscience*, *12*(9), 3433–3436.

Yan, J., Zhang, Y., Ehret, G. (2005). Corticofugal shaping of frequency tuning curves in the central nucleus of the inferior colliculus of mice. *Journal of Neurophysiology*, *93*(1), 71–83.

Yaron, A., Jankowski, M. M., Badrieh, R., Nelken, I. (2020). Stimulus-specific adaptation to behaviorally-relevant sounds in awake rats. *PLoS ONE*, *15*(3), 1–20.

Yu, Y.-Q., Xiong, Y., Chan, Y.-S., He, J. (2004). Corticofugal gating of auditory information in the thalamus: an in vivo intracellular recording study. *The Journal of Neuroscience : The Official Journal of the Society for Neuroscience*, *24*(12), 3060–3069.

Zacharias, N., König, R., Heil, P. (2012). Stimulation-history effects on the M100 revealed by its differential dependence on the stimulus onset interval. *Psychophysiology*, *49*(7), 909–919.

Zempeltzi, M. M., Kisse, M., Brunk, M. G. K., Glemser, C., Aksit, S., Deane, K. E., Maurya, S., Schneider, L., Ohl, F. W., Deliano, M., Happel, M. F. K. (2020). Task rule and choice are reflected by layer-specific processing in rodent auditory cortical microcircuits. *Communications Biology*, *3*(1), 1–12.

Zhao, L., Liu, Y., Shen, L., Feng, L., Hong, B. (2011). Stimulus-specific adaptation and its dynamics in the inferior colliculus of rat. *Neuroscience*, *181*, 163–174.

Declaration of honor

Hereby I declare to have written this thesis entitled “Layer specific adaptation in the primary auditory cortex of the Mongolian gerbil” all by myself. I have conducted all associated experiments during the time of my PhD at the Leibniz-Institute of Neurobiology. All used sources and used tools are enlisted. References have been cited appropriately.

Date of submission: 28.06.2021

Date of defense: 05.05.2022

Magdeburg, 14.07.2022 Jing Ma